Accepted Manuscript

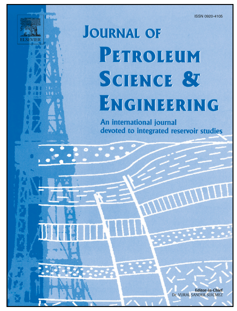

Diagenesis and reservoir quality of carbonates rocks and mixed siliciclastic as response of the Late Carboniferous glacio-eustatic fluctuation: A case study of Xiaohaizi Formation in western Tarim Basin

Mei-Yan Fu, Rong-Cai Song, Gluyas Jon, Shao-Nan Zhang, Qian Huang

PII: S0920-4105(19)30250-5

DOI: https://doi.org/10.1016/j.petrol.2019.03.011

Reference: PETROL 5861

To appear in: *Journal of Petroleum Science and Engineering*

Received Date: 5 June 2018

Revised Date: 13 February 2019

Accepted Date: 4 March 2019

Diagenesis and Reservoir Quality of Carbonates Rocks and Mixed siliciclastic as Response of the Late Carboniferous Glacio-Eustatic Fluctuation: A case study of Xiaohaizi Formation in Western Tarim Basin

FU MEI-YAN[1], SONG RONG-CAI[1*], JON GLUYAS[2], ZHANG SHAO-NAN[3], AND HUANG QIAN[1]

[1] *College of Energy Resources, Chengdu University of Technology, Chengdu 610059, China;*

[2.] *Department of Earth Science, Durham University, Durham, DH1 3LE, UK;*

[3] *College of Geosciences and Technology of Southwest Petroleum University, Chengdu 610500, China*

* Corresponding author: 417102145@qq.com

ABSTRACT: **Late Carboniferous-Permian was a longest-lived and most widespread ice age. The depositional environment, diagenesis and reservoir quality of carbonate rocks as response to the glacio-eustatic changes was analyzed in this study. The Upper Carboniferous Xiaohaizi Formation in the western Tarim Basin is an important oil reservoir. The dolostones from the Xiaohaizi Formation have very good physical properties, with maximum porosity and permeability of 16.6% and 214mD, respectively. The sedimentary facies of the Xiaohaizi Formation consist of carbonate shoals and lagoon on a mixed siliciclastic-carbonate platform. There was a strong heterogeneity of carbonate rocks deposited on shoals. Porous dolostones always alternate with tight sparry allochemical limestones. Based on the petrographic observation and stable isotope measurement, the controlling factors for the heterogeneity and reservoir quality were revealed. The palaeosol, vadose silt, karst breccia, detrital**

kaolinite, darkening of dolostones and enrichment of ^{18}O indicate the short-lasting subaerial emergence during the glacial period. During the glacial sea level fall, the mixed siliciclastic and carbonate allochems deposited on bioclastic and intraclastic shoals, while dolomitization of calcic grains occurred under a relatively low-temperature. Through the correlation analysis of physical property, lithology, rock components, it's suggested that the reservoir quality of the Xiaohaizi Formation was controlled by mixed sedimentation and dolomitization associated with glacio-eustatic fluctuation. At the burial diagenesis, the effect of hydrothermal fluid on physical properties of dolostones with relative high primary porosity was positive, whereas resulted in the poikilotopic calcite cementation. The assembly of fluorite, dickite and authigenic pyrite were indicators for hydrothermal fluid accumulation. The control of glacio-eustatic fluctuations on sedimentation and diagenesis in carbonates could be used to forecast the reservoir quality.

Keywords: **Carbonates; Mixed siliciclastic; Diagenesis; Reservoir Quality; Hydrothermal; Glacio-Eustatic**

INTRODUCTION

The glaciation successions on Gondwana supercontinent occurred at Carboniferous to Early Permian, resulting in glacio-eustatic sea level changes (Crowley and Baum 1991; Maynard and Leeder 1992; Butts 2005; Rygel et al. 2008; López-Gamundí and Buatois 2010). Assuming a constant rate of subsidence, glacio-eustatic sea level changes are recorded in the stacking patterns of facies and lithologies, e.g. the assembly of subtidal carbonate, mixed carbonate and siliciclastic, and quartz arenite (Butts 2005), as well as the subaerial exposure and meteoric diagenesis (Bishop et al. 2009; Elrick and Scott 2010), through waxing and waning of glaciation. A similar stratigraphy sequence of the Upper Carboniferous was found in the western Tarim Basin, northwestern China (Jiang and Gu 2002; Fu et al. 2012a). The main lithologies of gas zone from the Late Carboniferous in the western Tarim Basin are limestones and dolostones deposited on a carbonate platform (Zhang et al. 2009; Ma et al. 2015).

Based on the carbonate sequence associated with the sea-level fluctuation, the early diagenetic fabric and reservoir quality could have been influenced by the relative sea-level change (Sun and Esteban 1994; McKay et al. 1995; Strasser and Strohmenger 1997; Taghavi et al. 2006; Morad et al. 2012). The geochemical conditions of early diagenesis generally depend on the duration of relative sea-level changes (Morad et al. 2012). The subaerial exposure and meteoric diagenesis of carbonate rocks during glacio-eustasy in the mid-Late Carboniferous is an important diagenetic process that contributes to improve reservoir quality by enhancing both the porosity and permeability (Butts 2005; Bishop et al. 2009; Elrick and Scott 2010; Ueno et al. 2013). On the onset of glacio-eustasy, carbonate rocks experience subaerial emergence and chemical weathering in the ephemeral freshwater lenses, resulting in the formation of vugs, dissolve pores and calcite cementation (Strasser and Strohmenger 1997; Wang and Al-Aasm 2002; Hiatt and Pufahl 2014; Ren and Jones 2016). However, with the relative sea-level rise, dolomitization was prone to occur during transgressive system tract and early highstand system tract (Kordi et al. 2017). It has been suggested the dolomitization can be driven by sea water or modified sea water (Qing et al. 2001; Machel 2004). The pervasive dolomitization can be driven by periodically increased salinity response to relative sea-level fluctuation, assuming in a semiarid or arid environment (Sun and Esteban 1994). However, the diagenetic alteration and reservoir quality of carbonate rocks in response to the glacio-eustatic fluctuation in the Late Carboniferous in Tarim plate are poorly understood.

The impure carbonate rocks, containing a small amount of terrigenous detrital grains, occurred in the Upper Carboniferous Xiaohaizi Formation, the western Tarim Basin. The Carboniferous mixed sequence of dolostones, limestones, mudstones and sandstones resulted from the glacio-eustatic fluctuation in the study area (Fig.1)(Fu et al. 2012a). Based on the petrology and physical property, the mixed sedimentation and diagenesis related to the glacio-eustatic fluctuation were discussed, and then controlling factors for reservoir quality of these impure carbonate rocks were analyzed.

GEOLOGICAL SETTING

Tarim Basin is a typical superimposed basin in the Western China (Fig.1a) (Li et al. 1996). At the period of Carboniferous, the Tarim Plate drifted northward to a latitude of twenty degrees north (Jia 2013). Transgression after Ordovician began to inundate into the western Tarim Basin from west to east in the Early Carboniferous (Fu et al. 2012a). The multiple phases of eustatic fluctuation as the consequence of

Gondwanan glaciation (Rygel et al. 2008; López-Gamundí and Buatois 2010) during Carboniferous resulted in the formation of mixed siliciclastic and carbonate sequence in the western Tarim Basin (Fig.1) (Xiao and Pan 1999). At the Late Carboniferous, transgression reached to the zenith. Consequently, limestones deposited on the carbonate platform across the whole basin (Zhu et al. 2002; Jiang and Yu 2003; Ma et al. 2015).

During the Late Carboniferous to the Early Permian, the Tarim Plate appears to have collided with Siberia and Kazakhstan (Scotese and McKerrow 1990). Consequently, an extensive basalt eruption occurred during the Permian period (Ernst and Buchan 2001; Li et al. 2011). Meanwhile, the extensional tectonic movement significantly influenced the Tarim Basin, resulting in the oil and gas migration and hydrothermal fluid accumulation (Zhang et al. 2011a).

Bachu-Makit area is located in the western Tarim Basin, including Bachu uplift and Makit slope (Fig.1A). Makit slope is dipping southwest. Bachu uplift belongs to the western part of the central paleo-uplift (Song et al. 2018). Bachu-Makit area is closed to the Awati Depression, where is one of the hydrocarbon generation centers in the Tarim Basin (Zhang et al. 2011a). Several oil and gas fields have been discovered in the Carboniferous reservoirs in the Bachu-Makit area, such as Yasongdi Field, Bashituo Field, Niaoshan Field, and so on (Tan et al. 2004; Zhang et al. 2011b; Zhu et al. 2013; Song et al. 2018). Bachu-Makit area is one of the volcano activity centers in the Tarim Basin at the Early Permian (Meng et al. 2011). There are two deep fractures impenetrating from Cambrian to Permian (Li et al. 2015), e.g. Xianbazha fault and Selibuya fault (Fig.1B).

The Carboniferous lithologic units in the Bachu-Makit area include the Bachu, the Kalashayi and the Xiaohaizi formations (Fig.1C) from bottom to top. The Xiaohaizi Formation is an important oil bearing zone in the study area. The burial depth of the Xiaohaizi Formation ranges from 1944m to 4457m, with deeper depth from east to west. As the consequence of mixed sedimentation, quartz and clay mineral contents within carbonate rocks in the Xiaohaizi Formation are relatively high (Zhu et al. 2002; Fu and Zhang 2011).

MATERIAL AND METHODS

In this study, the cores of six wells were collected from Petroleum Exploration and Production Research Institute, Northwest Company, Sinopec Group, China. The core description was carried on more than 130 meters drilling cores from six wells (Table 1). The sedimentary structure, texture, color, and oil-bearing property were described on these cores. Based on the cores description, the macro-scale cycle of lithofacies was established (Fig.2).

179 thin sections were used for identification of mineralogy, diagenetic textures, and diagenesis. Thin sections were examined for mineralogy using Alizarin Red and potassium ferricyanide staining. Combining with the core description, the vertical changes of lithology on the stratigraphic column of the Xiaohaizi Formation were analyzed.

32 thin sections were observed under Cathode luminescence (CL), using CITL/CL8200 MK5-2 (made in England) cold cathode instrument. The voltage was 14 kV, and electric current is 380 μA. The CL images were captured with 20-second exposure times.

Scanning electron microscopy (SEM) petrography was performed using a Quanta 250 FEG (FEI Company, Hillsboro, OR, USA) with Oxford INCAx-max20 (Energy Disperse Spectroscopy, Oxford Instruments, Abingdon, England). These samples were coated with carbon, using secondary electron imaging. The resolution for secondary electron imaging under high vacuum is 2 nm, and that of backscattered electron imaging is 2.5 nm. The operating conditions were an accelerating voltage of 20kV, a filament current of 240μA, and beam diameter of 4 μm, and working distances of 10-20 mm.

A THMS 600 Cooling-Heating Stage (Linkam Scientific, Surrey, England) was used to measure the homogenization temperature (T_H) of fluid inclusion enclosed in the calcite cements. The temperature range of the instrument is from −196° to 600° C with a precision of <0.1 °C. The rate of temperature increase can be controlled to within 1 °C/min when approaching the critical point.

The composition of minerals was determined by using a Rigaku DMAX-3C x-ray diffractometer (Rigaku Corporation, Tokyo, Japan) equipped with Cu Kα radiation (40 kV, 20 mA). Angle accuracy is greater than 0.02° (2θ). The scanning speed was 0.05 s/step, and the scanning range was 3–50° (2θ). Semi-quantitative phase analysis was performed by a PDF2 (2004) computer using Jada 5.0 software. The relative deviation is less than 10% when the content of the mineral is more than 40%.

The composition of elements in carbonate rocks was detected by Optima 5300 V Inductively Coupled Plasma atomic emission spectroscopy (ICP-AES) (Perkin-Elmer Company) and Inductively Coupled Plasma mass spectrometry (ICP-MS). Aliquots of 100 mg of 13 bulk sample powders were dried at 100°C for two hours and dissolved in mixed solutions composed of 4 mL hydrofluoric acid, 2mL hydrochloric acid, 3mL nitric acid, 1mL perchloric acid and three drops of sulfuric acid. Then the samples dissolved in solutions were heated to about 200 °C for four hour until the white smoke occurring. The 5mL chloroazotic acids were added into the solutions to extract elements. The solutions were transferred to a 50mL volumetric flask, diluting with deionized water to volume. After that, the major elements were tested by ICP-AES and minor elements were tested by ICP-MS.

A total of 10 carbonate rocks from well M10 were measured for their bulk carbonate carbon and oxygen stable isotope values, measured by a MAT253 stable isotope ratio mass spectrometer (Thermo Scientific, Waltham, MA, USA). All the isotope data are reported as per-mil deviation from the Pee Dee Belemnite (PDB) standard. Samples were processed with phosphoric acid method. The measuring accuracy for ^{13}C is 0.0037‰, and that for ^{18}O is 0.013‰.

The gas method of Jannot and Lasseux (2012) was used to perform porosity and permeability tests. The relative deviation for porosity determinations is 0.5%–1.5% and that of permeability is ≤10% for low permeability samples.

RESULTS

Lithology, texture, and depositional characteristic

Lithology of the Xiaohaizi Formation in the study area comprises of calcitic marlstone, marly limestone, lime grainstone, partly dolomitized limestone and dolostones. There are two members of the Xiaohaizi Formation (Fig.2). The lithology of the upper member is dominantly argillaceous, marly limestone containing a very small amount of biodetritus and terrigenous siliciclastic grains. Marly limestone of the upper member deposited in the lagoon on a carbonate platform. In contrast, the lower member are characterised by granular dolostones and limestones, depositing on carbonate shoals. Besides the granular dolostone, the dolomicrite are observed in the interval. These dolomicrite composed of microcrystalline dolomites, occasionally with algal laminae, which deposited in the subtidal zone under a restricted marine environment.

Oil-bearing reservoirs are mainly composed of partly dolomitized limestones and granular dolostones in the lower member. These carbonate rocks are impure with a small amount of terrigenous detrital sands dominating by quartz. The content of terrigenous sands accounts for up to 10 vol. % of whole rock framework under microscope, occasionally 15 vol. % (Table 2). The composition of minerals determined by XRD shows that kaolinite accounts for 1-6 wt. % (Table 3). In addition, there is a small amount of pyrite.

The main textures of granular limestones are of grain-supported. The white limestones, with grain-supported texture are represented by intrasparite limestones, biosparite limestones and oospartie limestones. These carbonate rocks contain a wide array of bioclastic material including fusulinid, foraminifera, brachiopod, bivalve, echinodermata, and so on (Fig.3). The oncoids occasionally occurred within intraclastic limestones. The kernels of oncoids and ooids include the bivalve debris, echinodermata debris, and even quartz (Fig.3). These granular limestones deposited in different shoals, including intraclastic shoals, bioclastic shoals, and oolitic shoals. The dolomitization of grains is pervasive in limestones of intraclastic shoals and bioclastic shoals, resulting in the formation of partly dolomitized intrasparite/ biosparite limestones and finely crystalline granular dolostones. The crystal of dolomite is dirty and fine (Fig.3). The textures of granular dolostones are of grain-supported, but with the residual grain fabric and dark earthy yellow colour. The dissolved pores and vugs can be observed in the grain-supported dolostones. There are several discrete layers of dolostones alternating with undolomitized limestone at the lower member of the Xiaohaizi Formation (Fig.2). As a result, the lithologic heterogeneity occurs in the Xiaohaizi Formation.

The petrography of the granular dolostones shows some subaerial exposure features, including percolating clay, vadose silt, palaeosol, and karst breccia (Fig.4). The greyish-green percolating clay can be observed on cores. These percolating clays also can be seen under microscope. A very small amount of vadose silt filled in the moldic pores of biodetritus (Fig.4a), and karst breccia occurred in thin sections of well

BT8 (Fig.4b). The vadose silts have dark color, might be dyed by organic matters. The palaeosol as the weathering product occurred on cores from well BT3 (Fig.4c). The color of palaeosol was greyish-green, result from reduction during the diagenesis. The terrigenous elements enriched in dolostones adjacent to palaeosol layer, in terms of the concentration of terrigenous elements (Table 4).

Diagenetic Minerals

Calcite.-Calcite is the most abundant cement in the Xiaohaizi Formation. There are two generations of calcite cementation identified in sparry allochemical limestones (Fig.5). Based on the observation of thin sections, the first generation of calcite cementation occurs mainly as bladed calcite forming isopachous fringes on grains. The colour of bladed calcites under CL is dull, which is darker than the colour of grains (Fig.3ab). The second generation is of blocky spar, filling in the intergranular space (Fig.3c). The colour of blocky spar under CL is weak orange (Fig.3d). After alizarin Red and potassium ferricyanide staining, the colour of blocky calcite mostly becomes red, with very few mauve. The mauve colour shows the blocky spar comprised of a small amount of ferroan calcite.

The poikilotopic texture developed in granular dolostones, rather than the two generations of calcite cementation. Some partly dissolved dolomite crystals were embedded in poikilotopic calcites. The colours of poikilotopic calcites under CL are dull or dark orange (Fig.3d).

Micro-fractures are observed in biosparites and intrasparites, with two phases of calcite filling. The early calcites filled in the micro-fractures have bright orange CL colours, while the late calcites have very dark orange CL colours (Fig.3ef). In addition, the neomorphic calcites filled within bivalve's debris (Fig.3e).

Dolomite.-The dolomitization in the Xiaohaizi Formation resulted in the formation of micritic dolostones, partly dolomitized biosparite/intrasparite limestones, granular dolostones (Fig.5). The dolomite crystals of biogenic dolostones and intraclastic dolostones are euhedral, comprising of cloudy crystals with earthy yellow colour under plane-polarized light (Fig.5eg). Under CL, the colours of dolomites in these dolostones are dark red. The dolomitization of grains in granular dolostones is nearly complete, comprised of dolomitized grains and poikilotopic calcite cements. The dark earthy yellow colour of dolostones might be related to exposure, for the organic matter detected on the surface of dolomite (Fig.5h). The CL colours of dolomitized grains are dull (Fig.5e), implies different mechanisms with that of partly dolomitized grains. In addition, micritic dolomites as matrix are observed, with weak red CL colours (Fig.5).

Kaolinite and dickite.-Kaolinite and dickite are frequently observed in granular dolostones and limestones of the Xiaohaizi Formation. Kaolinite could form by chemical weathering or hydrothermal alteration of aluminosilicate minerals (Kerr 1952; Maliva et al. 1999). Blocky dickite is a polytype of kaolin, which can transform from vermiform kaolinite (Bailey 1980; Ehrenberg et al. 1993). Based on the observation of SEM, dickites have crystal size of 3-13μm (Fig.6a). The kaolinites or dickites distribute in the intergranular pores, dissolved pores (Fig.6a), intercrystalline pores of dolomite, and dissolved segment of stylolite. The CL colours of kaolinite and dickite are deep blue (Fig.6d). The identification of dickite by X-ray diffraction was published on our previous study (Fu et al. 2012b).

Fluorite.-A small amount of fluorite, mostly less than 1 vol. %, was observed in the dolostones from the Xiaohaizi Formation in well BT3, M4 and BT4 (Fig.6eg). Although the fluorite has not detected by XRD, there are a few fluorites in the sample from well BT4 at 4312.11m, with 2-3 vol. % of whole rock. The paradox is caused by the different samples with the same depth were tested by XRD and observed under microscope. Fluorites filled in the dissolved pores and micro-fractures, even growing as a euhedral crystal (Fig.6ef). Through observation under CL, the fluorites have bluish-violet CL colours, while some residual dissolved dolomites enclosed by the fluorite crystal (Fig.6g). In some thin sections, fluorite and dickites synchronously existed in dissolved pores (Fu et al. 2012b) (Fig.6g).

Pyrite.-Authigenic pyrite is occasionally observed in dolostones from the Xiaohaizi Formation. There is small amount of authigenic pyrites in well BT4 at 4312.11m under microscope (Fig.6h). However, the abundance of pyrite tested by XRD (see Table 3) is different with the result observed under microscope, which is caused by the different sample with the same depth. Using energy spectrum identification, authigenic pyrites filled in a large number of dissolved pores (Fig.6h). It implies that the authigenic pyrite postdating the late dissolution.

Overgrowth quartz.-The terrigenous quartz has experienced diagenetic alteration, including replacement, compaction/pressure dissolution and overgrowth. Overgrowth quartz was frequently observed in the porous dolostones containing fluorites and dickites. There were fine crystals of dolomite existing between detrital quartz and overgrowth quartz (Fig.6i). In sparry allochemical limestones, quartzes were prone to overgrows as euhedral crystal, while quartzes overgrew towards pores in porous dolostones.

Anhydrite/Gypsum.-Anhydrite or gypsum with plate like structure and bright interference colour occasionally can be observed in few samples, e.g. from well BT6 and BT8 (Fig.6j). The amount of anhydrite or gypsum is very few, only with less than 1 vol. % of whole rocks in two samples.

Carbon and oxygen stable isotope

The $\delta^{18}O_{-carbonate}$ of bulk carbonate ranges from -7.9‰ to 0.2‰PDB (Fig.7). There was an enrichment of ^{18}O during the global cooling in the Late Carboniferous-Permian (Veizer et al. 1999). There is an obvious vertical variation of $\delta^{18}O_{-carbonate}$ of Xiaohaizi Formation in well M10, might being related to the glacio-eustatic fluctuation. The shrift of dolostones to sparry allochemical limestones results in a 0.2‰ shift to more depleted $\delta^{18}O$ values of -7.4‰, as the boundary of glaciation and interglaciation (Fig.7). Meanwhile, the $\delta^{13}C$ values shift from -0.2‰ to 2.9‰ (Fig.7). There is obvious decrease of $\delta^{13}C$ values with $\delta^{18}O$ values.

Dissolution

The limestones and dolostones have experienced different phases of dissolution. There were three phases of dissolution. The first phase was the fabric selective dissolution, resulting in the formation of intragranular dissolved pores (Fig.8a). The second phase was the non-fabric selective dissolution. The dissolved pore was completely filled with blocky calcite (Fig.8b). The third one was the late dissolution, with development of intergranular dissolved pores and intercrystalline dissolved pore of dolomite without fillings (Fig.8c). Occasionally, dissolution of feldspar can be observed (Fig.8c). Dissolution gave rise to the generation of abundant pores in intraclastic or biogenic dolostones, creating a complicated pore network. There are also some intergranular pores observed in the granular dolostones and limstones without or very weak cementation (Fig.8d).

Physical properties

The lithologic heterogeneity results in various pore assemblies in carbonate reservoirs of the Xiaohaizi Formation. The lime grainstones, e.g. biosparite limestones and intrasparite limestones, generally have few visible pores (Fig.8). The two generations of calcite cements almost obstructed intergranular pores. The dissolved fractures and early non-fabric selective dissolved pores were fully filled with calcite (Fig.3). Few unfilled intergranular pores and intragranular pores developed in the granular limestones result in low porosity and permeability, with 0.4-2.5%, and 0.00-0.62mD, respectively (Fig.9). However, intrasparite limestones without cementation of blocky calcites (Fig.8d) have relative high porosity and permeability, with 8.5-14.8% and 5.33-39.5mD, respectively (Fig.9).

Dolostones develop more visible pores than limestones. Even so, the amount of pores in dolostones depends on the degree of dolomitization and cementation. The pores in dolostones are characterised by intergranular pores, intercrystalline pores, and dissolved pores. The partly dolomitized limestones with low degree of dolomitization have relative lower porosity and permeability than dolostones (2.5-5.8%, 0.01-2.16mD) (Fig.9). The porosity of dolostone was obviously influenced by poikilotopic calcite cementation. The dolostones without poikilotopic calcite have porosity of up to 16.6%, and permeability of up to 214mD (Fig.9).

DISCUSSION

Sedimentation on a mixed siliciclastic-carbonate platform

There are two sedimentary environments developed during the deposition of the Xiaohaizi Formation, including lagoon and carbonate shoals on a mixed siliciclastic-carbonate platform. As shown in Figure 2, the sedimentary environment of the Xiaohaizi Formation gradually changes from carbonate shoals to lagoon. The comparison among reservoir quality of rocks from different sedimentary facies is shown in Table 5. Marl limestones deposited in the lagoon with low hydrodynamic force are non-reservoir lithofacies. Within marl limestones, marl is the main element, with very few biodetritus and terrigenous detrital grains probably transported by storm waves. The pores within marl limestones were missing under microscope. Except the marl limestones with none visible porosity, the reservoir rocks deposited on the carbonate shoals include granular limestones, partly dolomitized limestones and granular dolostones. In terms of the physical properties of these rocks from the Xiaohaizi Formation, granular limestones with two generations of calcite cementation have fewest porosity than other three rocks (Fig.9). Some intraclastic limestones have only one generation of cementation, with more pores (Fig.8d). The partly or complete dolomitization in original biogenic limestones and intraclastic limestones results in the formation of porous dolostones reservoir, while there is no dolomitization observed in original oospartie limestones. Sum up, the reservoir rocks deposited on intraclastic shoals and biogenic shoals usually have a wide range from very poor to good physical properties (Table 5). The heterogeneity of physical properties comes from different diagenetic process (e.g. calcite cementation and dolomitization). However, the limestones deposited on oolitic shoals are always to be poor reservoirs. In addition, dolomicrite deposited on subtidal zone around shoals has low porosity with a very small amount of intercrystalline pores.

In terms of the observation and geochemical composition, there are a small amount of terrigenous siliciclastic grains and clay minerals inputting into the carbonate shoals (Table 2, 3, 4). In our previous study, the size distribution of quartz particles in the Xiaohaizi Formation shows the terrigenous materials deposited on the mixed carbonate shoals came from beach sands or aeolian sands (Fu et al. 2011). The siliciclast could be transported into carbonate platform by wind and current during mixed siliciclastic-carbonate sedimentation (Mount 1984; Fay et al. 1992; Brandano and Civitelli 2007). According to Fig.10a，the detrital quartz grains are prone to occur together with biodetritus (dominated by fusulinid and foraminifera) in sparry granular limestones (Table 2, Fig.10a). However, the contents of quartz within granular dolostone are relatively high, with up to 8% (Fig.7). The complete dolomitized grains in granular dolostones almost were the original intraclastic grains. It’s probably that there was relatively abundant quartz within original intraclastic limestones. Comparing with biodetritus and intraclast, the deposition environments of ooids and oncoids grains are little influenced by mixed siliciclastic-carbonate sedimentation. According to the content of terrigenous detrital quartz, the sedimentary facies on a mixed carbonate platform could be divided into mixed bioclastic and intraclastic shoals and normal shoals. The bioclastic and intraclastic shoals influenced by mixed sedimentation are proved to have highly reservoir quality with evidence from figure 10b.

The mixed sedimentation on the carbonate shoals could influence the physical property of reservoirs. The contents of terrigenous detrital quartz within carbonate rocks have a good positive relationship with their porosities (Fig.10c). In this study, the mixed sedimentation was regarded as the response to the glacio-eustatic fluctuations. There is a good correlation between content of detrital quartz and $\delta^{18}O_{-carbonate}$, as shown in Fig.7. Due to there was an enrichment of ^{18}O during the global cooling (Veizer et al. 1999), the increase of $\delta^{18}O_{-carbonate}$ verifies the onset of a glacial period. With the enhancement of glacial period, the sea level declined and the subaerial emergence occurred, with more input of terrigenous materials. The leaching of carbonate rocks by meteoric water during subaerial emergence could improve the physical property of reservoirs. Therefore, the mixed sedimentation related to glacio-eustatic fluctuations is an important factor controlling reservoir quality.

Diagenetic processes and subaerial diagenesis related to glacio-eustatic fluctuations

The diagenetic process of carbonate rocks from the Xiaohaizi Formation was established (Fig.11). The main diagenetic factors that influenced the reservoir quality include calcite cementation, subaerial exposure influenced by meteoric water, diagenesis related to hydrothermal fluid and dolomitization, as well as quartz overgrowth (Table 6). The effects of these diagenetic alterations on reservoir quality have been compared in Table 6. The dolomitization and dissolution related to meteoric water and hydrothermal fluid were the upmost important constructive diagenetic alteration, while calcite cementation destroyed the physical property.

There are different paths of paragenesis for sparry allochemical limestones and granular dolostones in the Xiaohaizi Formation (Fig.11). The cements of bladed high-magnesium calcite with dull CL colour around allochems and the framboidal pyrite occurred during early marine diagenesis. Under early diagenesis conditions, dolomitization of allochems predated the precipitation of bladed high-magnesium calcite. For complete dolomitized allochems, bladed calcite cements are absent. For the non-dolomitized limestone, the precipitation of blocky spars postdated the bladed cements to generate two phases of calcite cements. The two phases of calcite cements destructed the intergranular space among particles, resulting in the lowest porosity among granular limestones.

With evidence from petrography of dolostones and $\delta^{18}O_{\text{-carbonate}}$ of bulk carbonate analysis we can be sure that the diagenetic processes occurred during subaerial exposure, resulting from the glacio-eustatic sea level changes in the Late Carboniferous. During the sea-level fall as the result of glaciation with low CO_2, palaeosol formed after weathering of limestone and micritic carbonate minerals, and vadose silt filled in few pores during the subaerial exposure (Fig.4). The similar diagenetic alteration is reported elsewhere (Butts 2005; Ueno et al. 2013). In addition, granular dolostones have dark earthy yellow colours. The origin of the dark colour might be related to organic matter during exposure (Fig.6h) (Ueno et al. 2013). In the other hand, based on the vertical variation of $\delta^{18}O_{-carbonate}$, the positive apexes of $\delta^{18}O$ could represent the cold intervals during the glaciations (Fig.7). According to the fractionation of oxygen isotope, large amounts of ^{16}O water are being stored as glacial ice (Veizer et al. 1999). The generation of ice caps could have been the principal reasons for the observed ^{18}O enrichments. The upward trend to relative positive $\delta^{18}O$ values from interglaciation to glaciation in this study could be interpreted as a signal of long-term increase in salinity, being similar with the study of Mazzullo et al. (2007). There are some similar high frequency, moderate amplitude fluctuations in sea level during different periods when the globe is transitional between ice-house and green-house conditions, e.g. the Early/Late Ordovician, Early/Late Carboniferous boundary, Early/Late Permian boundary and parts of the early Neogene (Read and Horbury 1993).

However, the subaerial exposure of the lower member of the Xiaohaizi Formation lacks meteoric diagenetic fabric (Fig.4). The meniscus and dripstone cementation was absent. The lack of macro-scale karst or evidence of epidiagenesis suggests relatively short-lived exposure and/or a dry climate (Choquette and James 1988). Non-fabric selective dissolution occasionally occurred under inefficient meteoric diagenesis environment.

At the shallow burial process, dissolution occurred in porous dolostones experienced a very weak cementation in the early diagenesis. It’s suggested that the composition of mineral during ice-house times was mainly of global aragonite and high-Mg calcite (Sandberg1983), resulting in greater rates of early carbonate dissoloution. As a result, a large number of dissolved pores generated to increase the porosity further. After that, the pores without fillings in dolostones were partly filled by poikilotopic calcites. The kaolinite and overgrowth quartz precipitated after the feldspar dissolution. With particular hydrothermal fluid accumulated in porous dolostones along faults in some areas, authigenic minerals formed, e.g. fluorite, dickite and authigenic pyrite precipitated, as well as quartz overgrowth. Finally, with the oil charging, the diagenesis mostly ceased.

Occurrence and origin of kaolinite and dickite

The occurrence of authigenic kaolinite and dickite in carbonate rocks is related to chemical weathering, diagenesis, or hydrothermal fluid alteration (Schroeder and Hayes 1968; Jacka and Guven 1979; Maliva et al. 1999; Esteban and Taberner 2003; Fu et al. 2012b; Liu et al. 2016).

The formation of kaolin in the Xiaohaizi Formation was related to the dissolution of feldspar in the impure carbonate rocks, evidence from the petrography observation (Fig.8). The mix sedimentation of siliciclastic and carbonate minerals resulted in the input of terrigenous sands, including quartz, feldspar and lithic fragment. The kaolinite could form through meteoric water leaching both plagioclases and K-feldspars, under the subaerial environment, during early diagenesis or after structural inversion (Lanson et al. 2002). As a consequence of feldspar dissolution, kaolin precipitates according to:

$$\underset{\text{Feldspar}}{2KAlSi_3O_8} + 2H^+ + 9H_2O \leftrightarrow \underset{\text{Kaolinite}}{Al_2Si_2O_5(OH)_4} + \underset{\text{Silica}}{4H_4SiO_4} + 2K^+ \quad (1)$$

It's reported that there is a 5×10^6a depositional break at the end of Carboniferous (Xiao et al. 1995). As discussed above, there was subaerial emergence inside the Xiaohaizi Formation. However, the duration of exposure wouldn't last a long time. Scarcity of meteoric diagenetic fabrics and the occasional occurrence of gypsum in the study area indicate a less influence from meteoric water and a relative arid environment, just like the study of Triassic platform carbonate in a low latitude, tropical but arid setting (Christ et al. 2012). On the other hand, due to the amounts of siliciclastic grains within granular limestones and granular dolostones are very small (Table 2, 3), the input of feldspar during deposition period wouldn't be abundant. The insufficient meteoric water and a small amount of feldspar input resulted in the precipitation of kaolinite with content of less than 6% (Table 3). The detrital kaolinite deposited with allochems as the product of chemical weathering.

There is another hypothesis for the origin of diagenetic kaolin. CO_2-rich or organic acid-rich fluids may be responsible for feldspar alteration and subsequent precipitation of kaolin in buried sandstone (Ehrenberg 1991; Gaupp et al. 1993).

Kaolin can precipitate from the organic-rich pore water in limestones during burial diagenesis (Schroeder and Hayes 1968; Esteban and Taberner 2003; Fu et al. 2012b). In this study, the occurrence of kaolinite and dickite and overgrowth quartz synchronously existed in the finely crystalline biogenic and intraclastic dolostones with high visible porosity. The overgrowth quartz developed towards pores (Fig.6i), indicating the silica was supersaturated in the pore water of the Xiaohaizi Formation. Due to the relative high solubility of aluminum in organic acid-rich pore water (Maliva et al. 1999), the aluminum can be released by feldspar dissolution. In the study area, there are at least two times of oil charging, while the early oil charging occurred at Permian related to the Late Hercynian orogeny (Shao et al. 2010; Wang et al. 2015; Song et al. 2018). The intrusion of organic-acid predating oil charging resulted in the dissolution of feldspar, the precipitation of kaolin and the overgrowth of quartz. The partly dissolution of feldspar can be observed in thin sections (Fig.8c). The precipitation of vermiform kaolinite is also likely to occur in the burial diagenesis, resulting from *in situ* organic-acid dissolution of feldspar.

Dickite in the Xiaohaizi Formation can form through two pathways of diagenetic alteration (Fig.12). The kaolinite converted to dickite with increasing burial temperature (Lanson et al. 1996; Beaufort et al. 1998; Lanson et al. 2002; De Bona et al. 2008). Dickitization is of temperature-dependence, occurring at 100~130°C (Ehrenberg et al. 1993). However, it’s hard to explain the occurrence of dickite in well BT3 on the Bachu uplift with burial depth of 1944m, equivalent to 83 ºC (normal geothermal gradient 3 ºC/hm). According to the burial history of well BT4 in study area (Wang et al. 2015), the maximum burial depth of the Xiaohaizi Formation wouldn't be more than the depth at present. The low temperature of 83 ºC is not enough to cause dickitization of kaolinite. The hydrothermal activity in the study area probably is responsible for the dickitization. The high water/rock ratio during hydrothermal fluid accumulation is beneficial to dickitization (Lanson et al. 2002). The fluorite, as an indicator for hydrothermal fluid (Davies and Smith 2006), was also observed in the samples containing dickite (Fig.6). As a result, dickite mostly precipitated from hydrothermal fluid rather than transforming from kaolinite.

The effect of hydrothermal fluid on dolostone reservoirs

During the Early and Middle Permian, ultrabasic dyke was found in Bachu area resulting from the volcanic and igneous activity in Tarim Basin (Yang et al. 2007). The hydrothermal fluid migrates upwards along faults with volcanic activity. Few similar studies discussed the effect of hydrothermal fluid on dolostone reservoirs of the Xiaohaizi Formation in the study area (Fu et al. 2011, 2012b; Ma et al. 2015). In this study, evidence from the assembly of dickite, fluorite and authigenic pyrite indicated there was hydrothermal fluid activity. Fluorite postdated the precipitation of dickite. Authigenic pyrite formed in the dissolved pores as the react product of hydrothermal fluid rich in Fe^{2+} and H_2S. Sulfur could come from the underlying strata containing abundant gypsum (Fig.1). The homogenization temperatures of saline inclusions bearing hydrocarbon within calcite veins in well BT4 have the maximum value of 152.4°C (Fig.13), showing there was a high temperature resulting from hydrothermal fluid in the late diagenesis. The accumulation of hydrothermal fluid with high temperature and high water/rock ratio in dolostones could give rise to the formation of numerous dissolved pores, improving the physical property of reservoirs. Conversely, the precipitation of authentic minerals, e.g. fluorite, dickite, will fill with pores to decrease the porosity.

In the study area, a small amount of fluorite (mostly less than 1 vol. %) might imply the much less influence from hydrothermal fluid. The distribution of fluorite is strictly controlled by hydrothermal fluid. The porosity of dolostones containing fluorite is up to 13.5%, with average value of 9.7%. The abundant dissolved pores in dolostones without fillings indicate the possibility of late dissolution caused by hydrothermal fluid. The high primary porosity of dolostones facilitates the flow of hydrothermal fluid. The effect of hydrothermal fluid on physical property of dolostones with relative high primary porosity was positive.

However, the coarse crystalline poikilotopic calcite cements filled in pores of dolostones might result from hydrothermal fluid accumulation. The CL colour of poikilotopic calcite was dark orange (Fig.3bd), brighter than blocky calcite, showing a relative high concentration of Mn^{2+} (Hiatt and Pufahl 2014). As we know, meteoric water was the main source of manganese (Livingstone 1963). The input of Mn^{2+} has two potential sources including meteoric water and hydrothermal fluid. As discussed above, the arid palaeo-climate in the study area could result in less rainfall on the carbonate platform, leading to inefficient meteoric water diagenesis. Therefore, the high concentration of Mn^{2+} had relations with hydrothermal fluid rather than meteoric water in the early diagenesis. Fe^{2+} can quench luminescence (Hiatt and Pufahl 2014) to darken the luminescence. The precipitation of authentic pyrites could consume the spare Fe^{2+} from hydrothermal fluid. As a result, the relative brighter luminescence coarse crystalline poikilotopic calcite attributed to the relative high concentration of Mn^{2+} from hydrothermal fluid. The cementation following hydrothermal fluid accumulation could be the most deconstructive factor of physical property.

Dolomitization controls the reservoir quality

The physical property of the Xiaohaizi Formation is mainly controlled by dolomitization (as shown in Fig.9, Fig.10d). The earthy yellow dolomite crystals in these dolostones with fabric-retentive texture are characterised by small size, cloudy and euhedral-subhedral, with dark red colour under CL (Fig.5). The fabric-retentive texture shows the dolomitization occurred in the early diagenesis under low-temperature (Machel 2004). In this study, the porous dolostones alternated with tight limestone, caused by different degrees of dolomitization. The degrees dolomitization of allochems could be related to the surface-water circulation during sedimentation, through seawater evaporation (Machel 2004).

The multiple phases of eustatic fluctuation occurred in the Late Carboniferous, as the consequence of Gondwanan glaciation (Rygel et al. 2008; Buggisch et al. 2015). A similar study from Yangtze carbonate platform (China) in the Late Carboniferous-Early Permian, located in the similar palaeo-latitude with the study area, indicates the marine transgression and regression resulting from variations in the Gondwanan ice sheets (Ueno et al. 2013). The glacio-eustatic fluctuation caused the episodical restricted environment on carbonate shoals. In the restricted environment, the evaporation of active reflux brines can generate the mesohaline brines. However, seawater was below gypsum saturation during most of the complete dolomitization for the absence of gypsum precipitated in the study. The less negative δ^{13}C of whole carbonate rocks excludes the microbial or organogenic model of dolomitization. The darkening of dolostones also supports the subaerial emergence (Ueno et al. 2013). Although the mechanism of dolomitization is mysterious, we suggest that the change of sedimentary environment caused by glacio-eustatic fluctuation controlled the complete dolomitization during penecontemporaneous period.

Based on the petrography, the partial dolomitized grains were enclosed by isopachous bladed calcite, with brighter CL colour (Fig.5b,d) than completely dolomitized grains (Fig.5f). The formation of partial dolomitized grains might have another mechanism. Similar study speculated the reflux of gypsum-saturated brines could form discrete layers of dolostone that alternating with undolomitized limestone (Jones et al. 2003). The paragenesis represents a continuum of diagenetic processes resulting from progressive modification of diagenetic fluids. It’s credible that the latent reflux brines were responsible for the partial dolomitization at shallow burial stage, for the rare anhydrite occurred in the partly dolomitized intrasparite (Fig.6J).

Control of glacio-eustatic fluctuations on mixed sedimentation and diagenesis in carbonates and implications for forecasting reservoir quality

The mixed sedimentation and diagenetic processes inferred from petrographic observations and isotope analysis of the Xiaohaizi Formation are clearly linked to the glacio-eustatic conditions that existed in the area of what is now the Tarim Basin in the Late Carboniferous. The correlation between the content of terrigenous detrital quartz and $\delta^{18}O_{-carbonate}$, together with petrographic features under subaerial emergence, show the coincidence of sea level fall and mixed sedimentation. The granular dolostones deposited on mixed carbonate shoals have higher porosities than granular limestone on normal shoals. The suit of diagenetic minerals to occur as well as the absence of evidence for components like drip stones in these carbonate deposits indicates the importance of the predominantly cold, arid conditions during the exposure period (Read and Horbury 1993). It's clear that the reservoir quality of carbonate rocks in the Xiaohaizi Formation under cold and arid conditions was controlled by the mixed sedimentation and early diagenesis, especially dolomitization and weak cementation, as response to the sea level fall during glacial period. The depositional and diagenetic model of the Xiaohaizi Formation was established (Fig.14).

The limitations of this work stem principally from it being focused on a single basin in western China. It seems likely that carbonate strata of similar age in different locations around the globe should show some of the characteristic linked to sub-aerial exposure although it is likely that other locations will give an indication of humid rather than arid conditions. Further work on similar age carbonate sequences elsewhere in the world should enable a comprehensive understanding to be developed of the contemporaneous climate and sea-level conditions during the late Carboniferous. Moreover, given the impact the digenetic processes have had on improving reservoir quality in these carbonates, it should be possible once data from other basins are assembled, to construct a method whereby the quality of carbonate reservoir from the Late Carboniferous can be forecasted. This would be of significant value to both the petroleum and geothermal industries.

CONCLUSION

The reservoir quality of the Xiaohaizi Formation was controlled by mixed siliciclastic-carbonate sedimentation and dolomitization as response to glacio-eustatic fluctuation in the Late Carboniferous, with the contribution from subaerial exposure and partly from hydrothermal fluid alteration.

The lithology of the Xiaohaizi Formation gradually changes from granular limestones and dolostones deposited on carbonate shoals to marl limestones of lagoon. Discrete layers of porous dolostones alternating with tight undolomitized limestone within the shoal facies. It’s suggested that the mixed sedimentation could affect the reservoir quality, with evidence from the positive correlation between the content of terrigenous quartz and porosities of carbonate rocks. During glacial period, mixed sedimentation resulted in dolostones deposited on mixed shoals having higher porosities than that on normal shoals.

The dolostones have middle-high porosity and permeability, with maximum values of 16.6%, 214mD, respectively. The dolomitization of grains formed under low-temperature, which was related to episodical restricted environment. It’s clear that penecontemporaneous dolomitization and weak cementation controlled the reservoir quality, during subaerial exposure period. Evidences for the emergence of dolostones include vadose silt. palaeosol, karst breccia, detrital kaolinite, darkening of dolostones, and positive $\delta^{18}O_{\text{-carbonate}}$.

The contribution of hydrothermal fluid to the reservoir quality in the burial diagenesis was positive, although resulting in some poikilotopic calcite cementation. The assembly of fluorite, dickite and antigenic pyrite was the indicator of hydrothermal fluid accumulation. The dickite precipitated from hydrothermal fluid as the react product of feldspar dissolution under high temperature.

ACKNOWLEDGEMENTS

We thank Professor Huang Si-jing from Chengdu University of Technology for his constructive suggestion. We thank SinoPec of China for providing rock samples. We thank the State Key Laboratory of Oil and Gas Reservoir Geology and Exploitation in China for the measurement. The financial support of the research comes from the National Natural Science Foundation of China (Grant No. 41402096).

REFERENCES

Bailey, S.W., 1980. Structures of layer silicates, *in* Brindley, G. W. & Brown, G., eds., Crystal structures of clay mineral and their X-ray Identification: Monograph 5, Mineralogical Society, London, p. 1-123.

Beaufort, D., Cassagnabère, A., Petit, S., et al., 1998, Kaolinite-to-dickite conversion series in sandstone reservoirs: Clay Minerals, v. 33, p. 297-316.

Bishop, J. W., Montanez, I. P., Gulbranson, E.L., et al., 2009, The onset of mid-Carboniferous glacio-eustasy: Sedimentologic and diagenetic constraints, Arrow

Canyon, Nevada: Palaeogeography, Palaeoclimatology, Palaeoecology, v. 276.1, p. 217-243.

Brandano, M., and Civitelli, G., 2007, Non-seagrass meadow sedimentary facies of the Pontinian Islands, Tyrrhenian Sea: a modern example of mixed carbonate–siliciclastic sedimentation: Sedimentary Geology, v. 201.3, p. 286-301.

Buggisch, W., Krainer, K., Schaffhauser, M., et al., 2015, Late Carboniferous to Late Permian carbon isotope stratigraphy: A new record from post-Variscan carbonates from the Southern Alps (Austria and Italy): Palaeogeography, Palaeoclimatology, Palaeoecology, v. 433, p. 174-190.

Butts, S. H., 2005, Latest Chesterian (Carboniferous) initiation of Gondwanan glaciation recorded in facies stacking patterns and brachiopod paleocommunities of the Antler foreland basin, Idaho: Palaeogeography, Palaeoclimatology, Palaeoecology, v. 223.3, p. 275-289.

Choquette, P. W., James, N. P., 1988, Introduction, *in* James, N.P. and Choquette, P.W., eds., Paleokarst: Springer-Verlag, New York, p. 1–24.

Christ, N., Immenhauser, A., Amour, F., et al. 2012, Triassic Latemar cycle tops-Subaerial exposure of platform carbonates under tropical arid climate: Sedimentary Geology, v. 265, p. 1-29.

Crowley, T. J., and Baum, S. K., 1991, Estimating Carboniferous sea-level fluctuations from Gondwanan ice extent: Geology, v. 19.10, p. 975-977.

Davies, G. R. and Smith, J. L. B., 2006, Structurally controlled hydrothermal dolomite reservoir facies: an overview: AAPG Bulletin, v. 90, p. 1641–1690.

De Bona, J., Dani, N., Ketzer, J. M., et al., 2008, Dickite in shallow oil reservoirs from Recôncavo Basin, Brazil: diagenetic implications for basin evolution: Clay Minerals, v. 43.2, p. 213-233.

Ehrenberg, S. N., 1991, Kaolinized, potassium-leached zones at the contacts of the Garn Formation, Haltenbanken, mid-Norwegian continental shelf: Marine Petroleum Geology, v. 8, p. 250-269.

Ehrenberg, S. N., Aagaard, P., Wilson, M. J., et al., 1993, Depth-dependent transformation of kaolinite to dickite in sandstones of the Norwegian Continental shelf: Clay mineral, v. 28, p. 325-352.

Elrick, M., and Scott, L. A., 2010, Carbon and oxygen isotope evidence for high-frequency (10 4–105yr) and My-scale glacio-eustasy in Middle Pennsylvanian cyclic carbonates (Gray Mesa Formation), central New Mexico: Palaeogeography, Palaeoclimatology, Palaeoecology, v. 285.3, p. 307-320.

Ernst, R. E. and Buchan, K. L., 2001, Large mafic magmatic events through time and links to mantle-plume heads, *in* Ernst, R.E. and Buchan, K.L., eds., Mantle Plumes: Their Identification Through Time. Geological Society of America Special Paper 352, p. 483–575.

Esteban, M., and Taberner, C., 2003, Secondary porosity development during late burial in carbonate reservoirs as a result of mixing and/or cooling of brines: Journal of Geochemical Exploration, v. 78, p. 355-359.

Fay, M., Masalu, D. C. P., Muzuka, A. N. N., 1992, Siliciclastic—carbonate transitions in surface sediments of a back-reef lagoon north of Dar es Salaam (Tanzania): Sedimentary Geology, v. 78.1-2, p. 49-57.

Fu, M. and Zhang, S., 2011, Diagenesis of Quartz in Mixed Clastic-carbonate Rock and Its Relationship with Reservoir: Journal of Oil and Gas Technology, v. 33.12, p. 50-54 (Chinese, Abstract in English).

Fu, M., Zhang, S., Zhao, X., et al., 2012a, Researches of mixed sedimentation of the Carboniferous in Bachu-Makit area in Tarim Basin: Journal of Palaeogeography, v. 14.2, p. 155-164 (Chinese, Abstract in English).

Fu, M., Zhang, S., Hu, W., 2012b, The distribution and origin of dickite in carbonate: Acta Sedimentologica Sinica, v. 30.2, p. 310-317 (Chinese, Abstract in English).

Gaupp, R., Matter, A., Platt, J., 1993, Diagenesis and fluid evolution of deeply buried Permian (Rotliegende) gas reservoir, Northwest Germany: AAPG Bulletin, v. 77, p. 1111-1128.

Hiatt, E. E., and Pufahl, P. K., 2014, Cathodoluminescence petrography of carbonate rocks: a review of applications for understanding diagenesis, reservoir quality, and pore system evolution: Mineralogical Association of Canada, Short Course 45, Fredericton, New Brunswick, p. 75–96.

Jacka, A. D., and Guven, N., 1979, Occlusion of Porosity in Carbonate Reservoirs by Dickite: ABSTRACT: AAPG Bulletin, v. 63.3, p. 474-474.

Jannot, Y. and Lasseux, D., 2012, A new quasi-steady method to measure gas permeability of weakly permeable porous media. Review of Scientific Instruments, v. 8, p. 2015-2113.

Jia, C., 2013, Characteristics of Chinese petroleum geology: geological features and exploration cases of stratigraphic, foreland and deep formation traps: Springer Science & Business Media. p.15.

Jiang, L. and Gu, J., 2002, Analysis on the sedimentary environment of the carboniferous carbonate and detrital rock alternating sedimentation in the Maigaiti slope of the Tarim basin: Petroleum Geology & Experiment, v. 24.1, p. 41-47 (Chinese, Abstract in English).

Jiang, L., Yu, D., 2003, Research on Reservoir Characteristics of Carboniferous bioclast limestone member in Maigaiti Slope, Tarim Basin: Acta Scicentiarum Naturalum Universitis Pekinesis, v. 39.3, p. 428 - 434 (Chinese, Abstract in English).

Jones, G. D., Smart, P. L., Whitaker, F. F., et al., 2003, Numerical modeling of reflux dolomitization in the Grosmont platform complex (Upper Devonian), Western Canada Sedimentary Basin: AAPG Bulletin, v. 87, p. 1273–1298.

Kerr, P. F., 1952, Formation and occurrence of clay minerals: Clays and Clay Minerals, v.1.1, p. 19-32.

Kordi, M., Morad, S., Turner, B., et al., 2017, Sequence stratigraphic controls on formation of dolomite: Insights from the Carboniferous Um Bogma Formation, Sinai-Egypt: Journal of Petroleum Science and Engineering, v. 149, p. 531-539.

Lanson, B., Beaufort, D., Berger, G., et al., 1996, Late-stage diagenesis of clay minerals in porous rocks: Lower Permian Rotliegendes reservoir off-shore of The Netherlands: Journal of Sedimentary Research, v. 66, p. 501-518.

Lanson, B., Beaufort, D., Berger, G., et al., 2002, Authigenic kaolin and illitic minerals during burial diagenesis of sandstones: a review: Clay Minerals, v. 37, p. 1–22.

Li, D., Liang, D., Jia, C., Wang, G., Wu, Q., He, D., 1996, Hydrocarbons accumulations in the Tarim Basin, China: AAPG Bulletin, v. 80, p. 1587–1603.

Li, Z., Chen, H., Song, B., et al., 2011, Temporal evolution of the Permian large igneous province in Tarim Basin in northwestern China: Journal of Asian Earth Sciences, v. 42.5, p. 917-927.

Li, Y., Wen, L., Yang, H., et al., 2015, New discovery and geological significance of Late Silurian–Carboniferous extensional structures in Tarim Basin: Journal of Asian Earth Sciences, v.98, p. 304-319.

Liu, L. H., Ma, Y. S., Liu, B., et al., 2016, Hydrothermal dissolution of Ordovician carbonates rocks and its dissolution mechanism in Tarim Basin, China: Carbonates and Evaporites, p. 1-13.

Livingstone, D. A., 1963, Chemical composition of rivers and lakes, *in* Fleischer, M. eds., Data of Geochemistry: USA Reston Virgina, p. 41−44.

López-Gamundí, O. R., and Buatois, L. A., 2010, Introduction: Late Paleozoic glacial events and postglacial transgressions in Gondwana: Geological Society of America Special Papers, 468, v-viii.

MA, Z., YANG, S., XU, Q., et al., 2015, Main controlling factors of carbonate reservoirs of Xiaohaizi Formation in Xianbazha area, Tarim Basin: Petroleum Geology & Experiment, v. 37.3, p. 300-327 (Chinese, Abstract in English).

MACHEL, H. G., 2004, Concepts and models of dolomitization: a critical reappraisal: Geological Society, London, Special Publications, v. 235.1, p. 7-63.

MALIVA, R. G., DICKSON, J. A. D., and FALLICK, A. E., 1999, Kaolin cements in limestones: potential indicators of organic-rich pore waters during diagenesis: Journal of Sedimentary Research, v. 69, p. 158-163.

MAYNARD, J. R., and LEEDER, M. R., 1992, On the periodicity and magnitude of Late Carboniferous glacio-eustatie sea-level changes: Journal of the Geological Society, v. 149.3, p. 303-311.

MAZZULLO, S. J., BOARDMAN, D. R., GROSSMAN, E. L., et al., 2007, Oxygen-carbon isotope stratigraphy of Upper Carboniferous to Lower Permian marine deposits in Midcontinent USA (Kansas and ne Oklahoma): Implications for sea water chemistry and depositional cyclicity: Carbonates and Evaporites, v. 22.1, p. 55-72.

MCKAY, J. L., LONGSTAFFE, F. J., and PLINT, A. G., 1995, Early diagenesis and its relationship to depositional environment and relative sea‐level fluctuations (Upper Cretaceous Marshybank Formation, Alberta and British Columbia): Sedimentology, v. 42.1, p. 161-190.

MENG, Q., ZHU, D., XIE, Q., et al., 2011, Controlling factors for deep fluid activity and prediction of positive effect area in middle Tarim and Bachu region: Petroleum Geology &Experiment, v. 33.6, p. 597-606.

Morad, S., Ketzer, J. M., De Ros, L. F., 2012, Linking Diagenesis to Sequence Stratigraphy: An Integrated Tool for Understanding and Predicting Reservoir Quality Distribution, *in* MORAD, S., KETZER, J. M., DE ROS, L. F., eds., Linking Diagenesis to Sequence Stratigraphy. International Association of Sedimentologists, Special Publication, v. 45, p. 1–36.

Mount, J. F., 1984, Mixing of siliciclastic and carbonate sediments in shallow shelf environments: Geology, v. 12, p. 432-435.

Qing, H., Bosence, D. W. J., and Rose, E. P. F., 2001, Dolomitization by penesaline sea water in Early Jurassic peritidal platform carbonates, Gibraltar, western Mediterranean: Sedimentology, v. 48.1, p. 153-163.

Read, J.F., and Horbury, A.D., 1993, Eustatic and tectonic controls on porosity evolution beneath sequence-bounding unconformities and parasequences disconformities on carbonate platforms. *in* HORBURY, A.D., and ROBINSON, A.G., eds., Diagenesis and basin development, American Association of Petroelum Geologists Studies in Geology #36, p. 155-197.

Ren, M., and Jones, B., 2016, Diagenesis in limestone-dolostone successions after 1 million years of rapid sea-level fluctuations: A case study from Grand Cayman, British West Indies: Sedimentary Geology, v. 342, p. 15-30.

Rygel, M. C., Fielding, C. R., Frank, T. D., et al., 2008, The magnitude of Late Paleozoic glacio-eustatic fluctuations: a synthesis: Journal of Sedimentary Research, v. 78.8, p. 500-511.

Sandberg, P.A., 1983, An oscillating trend in Phanerozoic non-skeletal carbonate mineralogy: Nature, v. 305, p. 19-22.

Schroeder, R. J., and Hayes, J. B., 1968, Dickite and kaolinite in Pennsylvanian limestones of southeastern Kansas: Clays and Clay Minerals, v. 16, p. 41-49.

Scotese, C. R., and McKerrow W. S., 1990, Revised world maps and introduction: Geological Society, London, Memoirs, v. 12.1, p. 1-21.

Shao, Z., Lv, H., and Geng, F., 2010, Geochemical characteristics of the Carboniferous oil pools in Maigaiti area, the Tarim Basin: Oil & Gas Geology, v. 31.1, p. 84-90 (Chinese, Abstract in English).

Song, D., Shi, L. S. Han, Z. and Meng B., Geochemistry and possible origin or crude oils from Bashituo Oilfield, Tarim Basin, (*in press; preliminary version published online Ahead of Print* 31 October 2018): AAPG Bulletin, doi:10.1306/10031817403.

Strasser, A., and Strohmenger, C., 1997, Early diagenesis in Pleistocene coral reefs, southern Sinai, Egypt: response to tectonics, sea−level and climate: Sedimentology, v. 44.3, p. 537-558.

Sun, S.Q., and Esteban, M., 1994, Paleoclimatic controls on sedimentation, diagenesis, and reservoir quality: lessons from Miocene carbonates: AAPG bulletin, v. 78.4, p. 519-543.

Taghavi, A.A., Mørk, A., and Emadi, M.A., 2006, Sequence stratigraphically controlled diagenesis governs reservoir quality in the carbonate Dehluran Field, southwest Iran: Petroleum Geoscience, v. 12.2, p. 115-126.

Tan, K., Mu, Z., Lv, X., et al., 2004, The exploration potential of oil and gas of the carboniferous system in the Tarim southwest area: Natural Gas Geoscience, v. 15.12, p. 115-115 (Chinese, Abstract in English).

Ueno, K., Hayakawa, N., Nakazawa, T., et al., 2013, Pennsylvanian–Early Permian cyclothemic succession on the Yangtze Carbonate Platform, South China: Geological Society, London, Special Publications, v. 376.1, p. 235-267.

Veizer, J., Ala, D., and Azmy, K., et al., 1999, $^{87}Sr/^{86}Sr$, $\delta^{13}C$ and $\delta^{18}O$ evolution of Phanerozoic seawater: Chemical geology, v. 161.1, p. 59-88.

Wang, B., and Al-Aasm, I.S., 2002, Karst-controlled diagenesis and reservoir development: Example from the Ordovician main-reservoir carbonate rocks on the eastern margin of the Ordos basin, China: AAPG bulletin, v. 86.9, p. 1639-1658.

Wang, X., Feng, Y., and Cao, Z., 2015, Application of various aspects of fluid inclusions in hydrocarbon formation history, taking Bachu-Maigaiti area of Tarim Basin as an example: Journal of Northeast Petroleum University, v. 39.2, p. 26-33(Chinese, Abstract in English).

Xiao, C., Li, L., Jiang, Y., et al., 1995, The Discovery Of Sedimentary Hiatus In Xiaohaizi Formation In Xiaohaizi Area, Bachu, Xinjiang And Its Geological Significance: Petroleum Exploration and Development, v. 22.3, p. 54-57 (Chinese, Abstract in English).

Xiao, C., and Pan, Y., 1999, Carboniferous Mixed Terrigenous Clastic, Carbonate and Sulphate Sediments in the Bachu Area, Xinjiang: Acta Geologica Sinica (English Edition), v. 73.3, p. 341-347.

Yang, S., Yu, X., Chen, H., et al., 2007, Geochemical characteristics and petrogenesis of Permian Xiaohaizi ultrabasic dyke in Bachu area, Tarim basin: Acta Petrologica Sinica, v. 23.5, p. 1087-1096 (Chinese, Abstract in English).

Zhang, R., Feng, Q., Zhang, H., et al., 2009, Characteristics and Control Factors of Carboniferous Bioclast Limestone Member Reservoir in the Qunkuqiake Area, Tarim Basin: ACTA GEOLOGICA SINICA, v. 83.4, p. 590-598 (Chinese, Abstract in English).

Zhang, S., Zhang, B., Li, B., et al., 2011a, History of hydrocarbon accumulations spanning important tectonic phases in marine sedimentary basins of China: Taking the Tarim Basin as an example: Petroleum Exploration and Development, v. 38.1, p. 1-15.

Zhang, Z., Liu, S., Yang, Z., et al., 2011b, Tectonic evolution and its petroleum geological significances of the Maigaiti Slop, Tarim Basin: Oil&Gas Geology, v. 32.6, p. 909-919 (Chinese, Abstract in English).

Zhu, R., Luo, P., and Luo, Z., 2002, Lithofacies palaeogeography of the late Devonian and carboniferous in Tarim basin: Journal of Palaeogeography, v. 4.1, p. 13-24 (Chinese, Abstract in English).

Zhu, G., Zhang, S., Su, J., et al., 2013, Secondary accumulation of hydrocarbons in Carboniferous reservoirs in the northern Tarim Basin, China: Journal of Petroleum Science and Engineering, v. 102, p. 10-26.

FIGURES CAPTIONS

Fig.1 (a). Location of the Bachu-Makit area in the western Tarim Basin; **(b)**. The distribut on of oil and gas field in the Bachu-Makit area; **(c).** The stratigraphic column of Carboniferous in the Bachu-Makit area.

Fig.2 Stratigraphic column and sedimentary environments of the Upper Carboniferous Xiaohaizi Formation in well BT4.

Fig.3 Lithology of the Xiaohaizi Formation. **(a).** Intrasparite limestone containing ooids, intraclast, and bioclast under plane-polarized light. The dark colours of grains were related to organic matters. The two generations of calcite cementation obstruct nearly all visible pores. **(b).**The image of (a) under cathode luminescence (CL). Note the CL colours of two generations of calcite cements are different. The early bladed calcites are non-luminescent, while the late blocky spars are dull orange. **(c)**.Fine crystalline intraclastic dolostone, cemented by poikilotopic calcite, under plane-polarized light. The crystals of dolomite are dull yellow. **(d)**.The image of (c) under CL. The CL colours of complete dolomitized grains are subtle null, while the poikilotopic calcites have dark orange colours. **(e)**. Intrasparite limestone with two phases of micro-fractures, under plane-polarized light. **(f)**. the image of (e) under CL. The CL colours of early micro-fractures are bright orange, while that of the late fracture are dark orange.

Fig.4 The features of subaerial exposure. **(a).** Vadose silt filled in the moldic pores of bioclast. VS-vadose silt. **(b).** Weathering breccia in intrasparite limestone, cemented by calcites. Br-breccia. **(c).** Several palaeosol layers on the brecciated dolostone in the lower Xiaohaizi Formation, indicated by yellow arrows. **(d)**. SEM image of clay minerals among dolomites.

Fig.5 The features of dolomitization in the Xiaohaizi Formation. **(a)**.Dolomitic intrasparite limestone with partly dolomitized grains, under plane-polarized light. The crystals of dolomite inside grains are dirty and fine. The two generations of calcite cements obstructed nearly all visible pores. Cc-calcite; Cc-I-the first generation of calcite; Cc-II-the second generation of calcite; **(b)**. The image of (a) under cathode luminescence (CL). Partially dolomitized grains have dark red colours under CL, minor dark orange. The CL colours of early bladed calcites are dull, caused by very low Mn^{2+}. The late blocky calcites have dark orange colours under CL, indicating a low Mn^{2+} or high Fe^{2+} diagenetic environment. **(c).** Dolomitic intramicrite, under plane-polarized light. The grains have partly dolomitized, while the matrix is completely dolomitized. The bladed calcites grow around grains as isopachous fringes. **(d).** The image of (c) under CL. The partly dolomitized grains have weak orange colours. The colours of bladed calcite are null, while the micritic dolomites have weak red colours. **(e)**. Intraclastic dolostone, under plane-polarized light. The dolomitized grains are dark earthy yellow. Poikilotopic calcites and fluorites fill in the pores. **(f).** The image of (e) under CL. The colours of complete dolomitized grains are subtle dull, indicating a very low Mn^{2+} environment. Poikilotopic calcites have dark to bright orange colours. The fluorites have deep blue colours. **(g)**. The SEM image of dolomitized grains, with the crystal size ranging from14-32μm. **(h).** The SEM image of organic matters among dolomites. These organic matter contain abundant C, N, O, belonging to the component of palaeosol. OM-organic matter.

Fig.6 The photos of diagenetic minerals in the Xiaohaizi Formation. **(a).** The SEM image of dickites. The blocky dickite crystals, with size of 3-13μm, have the spatial organization seems inherited from pre-existing booklets. **(b).** The image of kaolinites filling in intergranular dissolved pores among dolomitized grains, under plane-polarized light. Blue areas are pores. **(c).** Dickites fill within intergranular dissolved pores, under cross-polarized light. Dickites have interference colour of greyish white. **(d).** The image of (c) under cathode luminescence (CL). Dickites have deep blue colours under CL. The dissolved dolomites were enclosed by dickites. **(e).** Euhedral crystal of fluorite grows in dolostone. Opaque pyrites are oserved. **(f).** The image of (e) under CL. The colour of fluorite is bluish-violet. **(g).** The image of fluorites and dickites under CL, from Fu et al., 2012b. The dickites were enclosed in fluorites, indicating precipitation of fluorites postdated dickites. **(h).** The SEM image of pyrite on thin section. Authigenic pyrite filled in the dissolved pores, postdating dissolution. **(i).** The image of overgrowth quartz under cross-polarized light. The overgrowth quartz grows towards intergranular pores. It shows quartz overgrowth occurred after compaction. There are fine crystals of dolomite existing between detrital quartz and overgrowth quartz. **(j).** The image of anhydrite in the partly dolomitized intrasparite under cross-polarized light. The bright interference colour and plate like structure can be identified as anhydrite.

Fig.7 The vertical variation of content of terrigenous quartz, carbon and oxygen isotope of the Xiaohaizi Formation in well M10. Note that there are two cycles of inter-glaciation period and glaciation period. The high content of quartz and enrichment of ^{18}O stands for the onset of glacial period.

Fig.8 The photos of different types of pores in the Xiaohaizi Foramtion. **(a).** The image of intragranular pore under plane-polarized light. **(b).** The non-fabric selective pores filled with calcite, under plane-polarized light. **(c).** The image of dissolved intergranular pores, under plane-polarized light. Paritally dissolved feldspar (yellow arrow) is present. **(d).** The image of primary intergranular pores in intrasparite, under plane-polarized light. DIP: dissolved intergranular pore; IP: intergranular pore; IAP: intragranular pore; Cc: calcite; Do: dolomite.

Fig.9 The cross plots of porosity and permeability. (a).The bulk data for all samples. There is a good positive correlation, with coefficient of 0.7677. **(b).** The relationship between lithology and physical property. The dolostones have highest porosity and permeability than other rocks.

Fig.10 The correlation analysis of physical property, lithology and rock components. **(a).** The cross plot of terrigenous grains contents and biodetritus contents within whole rock; **(b).** The porosities of reservoir rocks from different microfacies of carbonate shoals; **(c).** The cross plot of porosities of reservoir rocks and contents of detrial quartz within whole rock; **(d).** The cross plot of porosities of reservoir rocks and contents of dolomite within whole rock.

Fig.11 Paragenesis of the carbonate rocks from the Xiaohaizi Formation.

Fig.12 The transformation pathway of kaolinite and dickite in the Xiaohaizi Formation.

Fig.13 The homogeneous temperatures of fluid inclusions within the calcite veins of the Xihaozi Formation in well BT4.

Fig.14 The depositional and diagenetic model of the Xiaohaizi Formation during the cycle of interglaciation and glaciation. The mixed siliciclastic-carbonate sedimentation and subaerial exposure controls the formation of porous dolostones, as response to the sea level fall with proceeding of glaciation. Dolostones with weak cementation have abundant pores to be the best reservoir rocks.

Table 1 The information of drilling cores from the Xiaohaizi Formation in six wells

Well	Length of cores (m)	Top depth (m)	Bottom depth (m)
BT4	18.92	4301	4319.92
BT8	52.17	4483.53	4535.7
M10	37.42	4394	4431.42
BT3	15.89	1911.42	1927.31
BT6	16.12	4438.6	4454.72
M4	5.4	4385.5	4390.9

Table 2 The content of components in part of carbonate rocks from the Xiaohaizi Formation

Well	Depth (m)	Lithology	Content of component (vol. %)							Assembly of creatures
			intraclastic	bioclastic	oncoid	ooid	terrigeous detrital grain	micrite matrix	cement	
BT4	4301.64	Oosparite limestone	25	10	5	35	/	/	25	echinodermata, bryozoan,brachiopod
BT4	4302.16	Biosparite limestone	10	56	/	/	4	/	30	green algae,fusulinid, echinodermata, brachiopod
BT4	4302.87	Biosparite limestone	8	59	/	/	8	/	25	fusulinid, echinodermata, brachiopod
BT4	4308.63	Intrasparite limestone	45	25	/	/	/	/	30	fusulinid, echinodermata, brachiopod
BT4	4304	Biosparite limestone	5	60	/	/	10	/	25	foraminifera, echinodermata, brachiopod
BT4	4315.24	Intrasparrudite limestone	55	20	/	/	/	/	25	fusulinid, echinodermata, brachiopod
BT8	4483.03	Biomicrite	/	65	/	/	/	35	/	foraminifera, echinodermata, brachiopod
BT8	4484.12	Biosparite limestone	30	40	10	/	/	/	20	echinodermata,green algae,brachiopod, foraminifera,bryozoan,gastropods
BT8	4493.24	Partly dolomitized oosparite limestone	15	5	/	51	1	/	28	brachiopod,bivalve, echinodermata
BT8	4495.95	Partly dolomitized intrasparite limestone	71	4	/	/	/	/	25	echinodermata,brachiopod,green algae,fusulinid

Table 3 The composition of minerals determined by XRD from the Xiaohaizi Formation

Well	Depth （m）	Lithology	Content of minerals (wt.%)					
			Kaolinite	Quartz	Calcite	Dolomite	Pyrite	Anhydrite
M10	4397.30	dolostone	/	1	3	96	/	
M10	4398.10	calcareous dolostone	2	2	33	63	/	
M10	4400.10	calcareous dolostone	1	2	27	70	/	
M10	4406.54	calcareous dolostone	/	/	25	75	/	
M10	4404.94	calcareous dolostone	/	/	21	79	/	
BT4	4312.11	dolostone	6	/	9	84	1	
BT3	1918.02	dolostone	/	1	2	97	/	
BT3	1921.48	calcareous dolostone	1	1	48	50	/	
BT3	1924.11	limestone	1	3	95	1	/	
BT3	1924.11	limestone	1	3	96	/	/	

/: none

Table 4 The composition of terrigenous elements in carbonate rocks from the Xiaohaizi Formation

Well	Depth(m)	Position of sample	Concentration of elements (μg/g)						
			Al	Sr	Ba	Ti	Cr	Rb	K
BT3	1924.11	adjacent to palaeosol	9619.01	463.49	243.01	225.67	9.17	8.89	2171.52
	1924.11		9415.54	509.80	665.88	236.82	10.47	10.11	1907.77
	1924.11		7262.50	384.00	233.50	251.00	18.50	25.62	2300.25
BT3	1918.02	undersea	4993.07	118.88	11.15	48.79	5.94	1.62	351.69
BT4	4306.93		6792.48	207.07	16.62	99.20	30.01	2.36	586.50
BT4	4312.11		6555.00	174.50	44.50	193.75	23.25	3.69	643.00
BT4	4316.09		3698.15	268.37	178.41	37.73	7.75	0.96	327.09
BT4	4217.55		3880.00	220.50	6.25	46.50	22.50	\	535.25
M10	4397.30		4480.00	673.50	11.75	95.00	12.00	3.27	494.75
M10	4398.10		6016.59	166.37	20.11	120.43	27.81	1.45	640.40
M10	4400.10		5260.00	176.25	8.50	107.00	26.75	2.06	344.75
M10	4404.94		3400.00	167.25	3.00	45.75	10.25	1.04	152.25
M10	4406.54		5315.00	158.50	29.25	47.75	10.00	1.66	354.00

Table 5 Summary chart of the petrologic characteristic in different depositional environments

Depositional facies			Lithology	Color	Structure	Texture	Physical property	Porosity(%)
Facies	Sub-facies	Mirco-facies						
mixed siliciclastic-carbonate platform	lagoon	Marl	Marly limestone	Dark grey	Fracture	Matrix-supported	Extreme Poor	none
	Carbonate shoal	Bioclastic shoal	Biosparite limestone, biogenic dolostones, partly dolomitized biosparite limestone	White	Stylolite, vug	Grain-supported	Very Poor-Very good	0.8-13.5
		Oolitic shoal	Oosparite limestone，	White	Fracture, stylolite	Grain-supported	Very Poor	1.2-2.0
		Intraclastic shoal	Partly dolomitized intrasparite limestone, finely crystalline intraclastic dolostones	Yellow grey, dark earthy yellow	Fracture, vug	Grain-supported, residual grain fabric	Very Poor-Very good	0.4-16.6
		Subtidal zone	Dolomicrite	Grey	Laminar algal	Microcrystalline	Very Poor-Poor	0.8-7.4

Table 6 Summary chart of the main diagenesis and their effect on reservoir quality

Type of main diagenesis	Diagenetic mineral	Diagentic environment	Supporting evidence	Effect on reservoir quality
Early calcite cementation	Bladed calcite, blocky calcite,	Sea water	Dull and weak organce CL color	Destructive
Dissolution by meteoric water	Blocky calcite, kaolinte	Subaerial exposure	Vadose silt, palaeosol	Constructive
Dissolution and cementation related to hydrothermal fluid	Fluorite, pyrite, dickite, poikilitic calcite	Hydrothermal fluid	Assembly of fluorite, pyrite, and dickite; High TH ,high concentration of Mn^{2+}	Constructive /destructive
Dolomitization	Dolomite	Low-temperature, episodical restricted environment; Shallow buried	Small, euhedral and cloudy crystals, dull to dark red CL color	Constructive
Quartz overgrowth	Overgrowth quartz	Moderate to deep buried	Euhedral crystal	Irrelevant/destructive

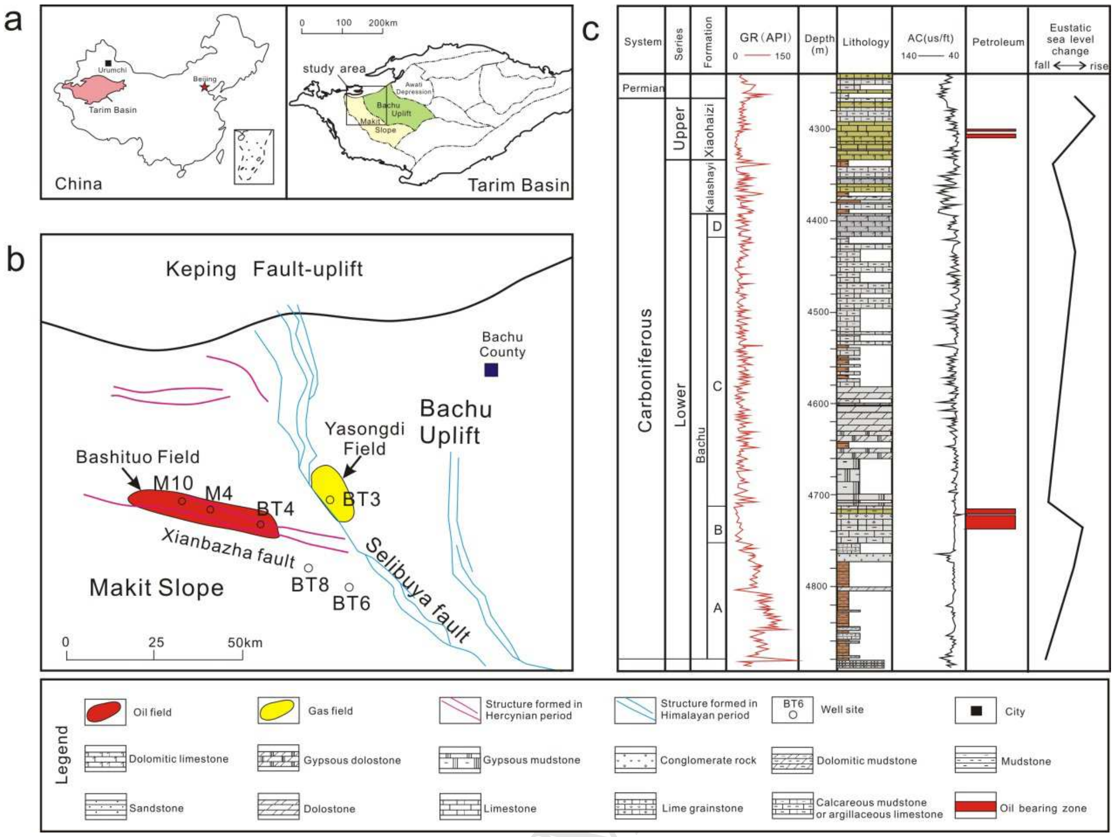

Fig.1 (a). Location of the Bachu-Makit area in the western Tarim Basin; **(b).** The distribut on of oil and gas field in the Bachu-Makit area; **(c).** The stratigraphic column of Carboniferous in the Bachu-Makit area.

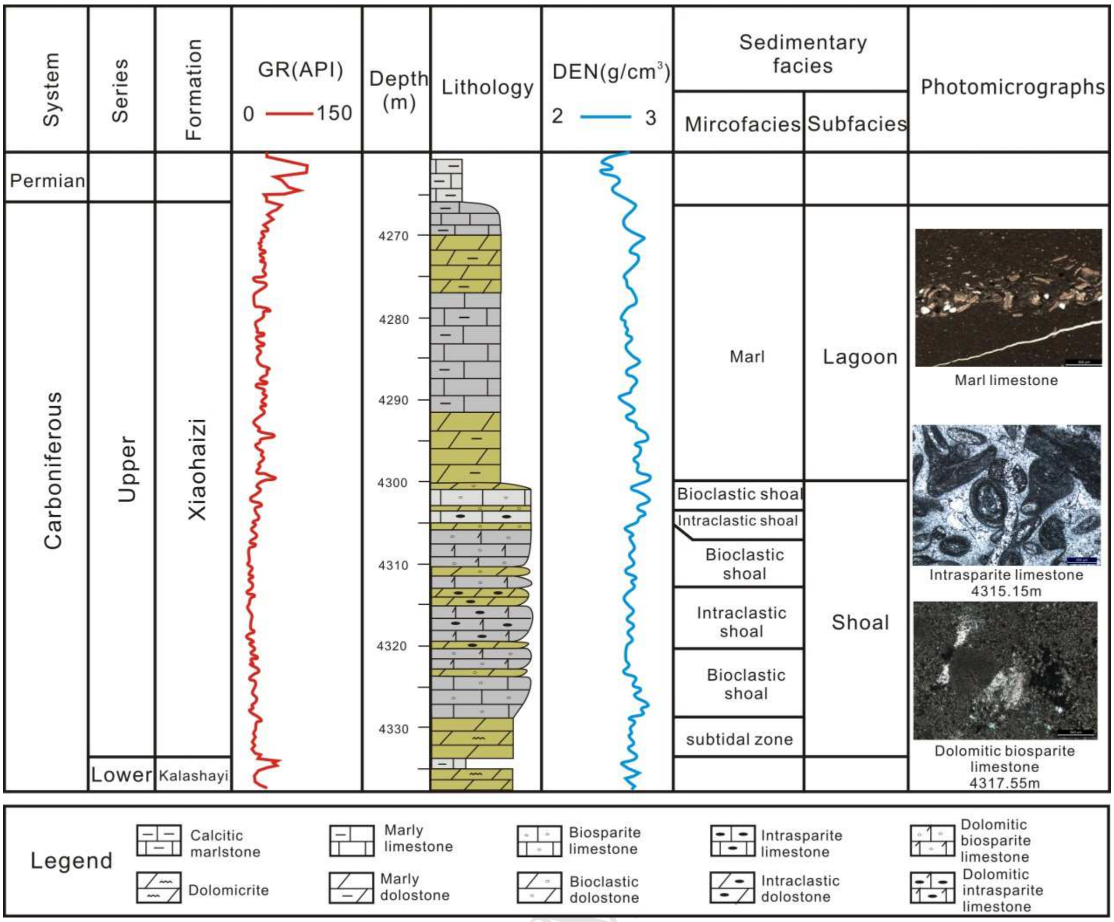

Fig.2 Stratigraphic column and sedimentary facies of the Upper Carboniferous Xiaohaizi Formation in well BT4.

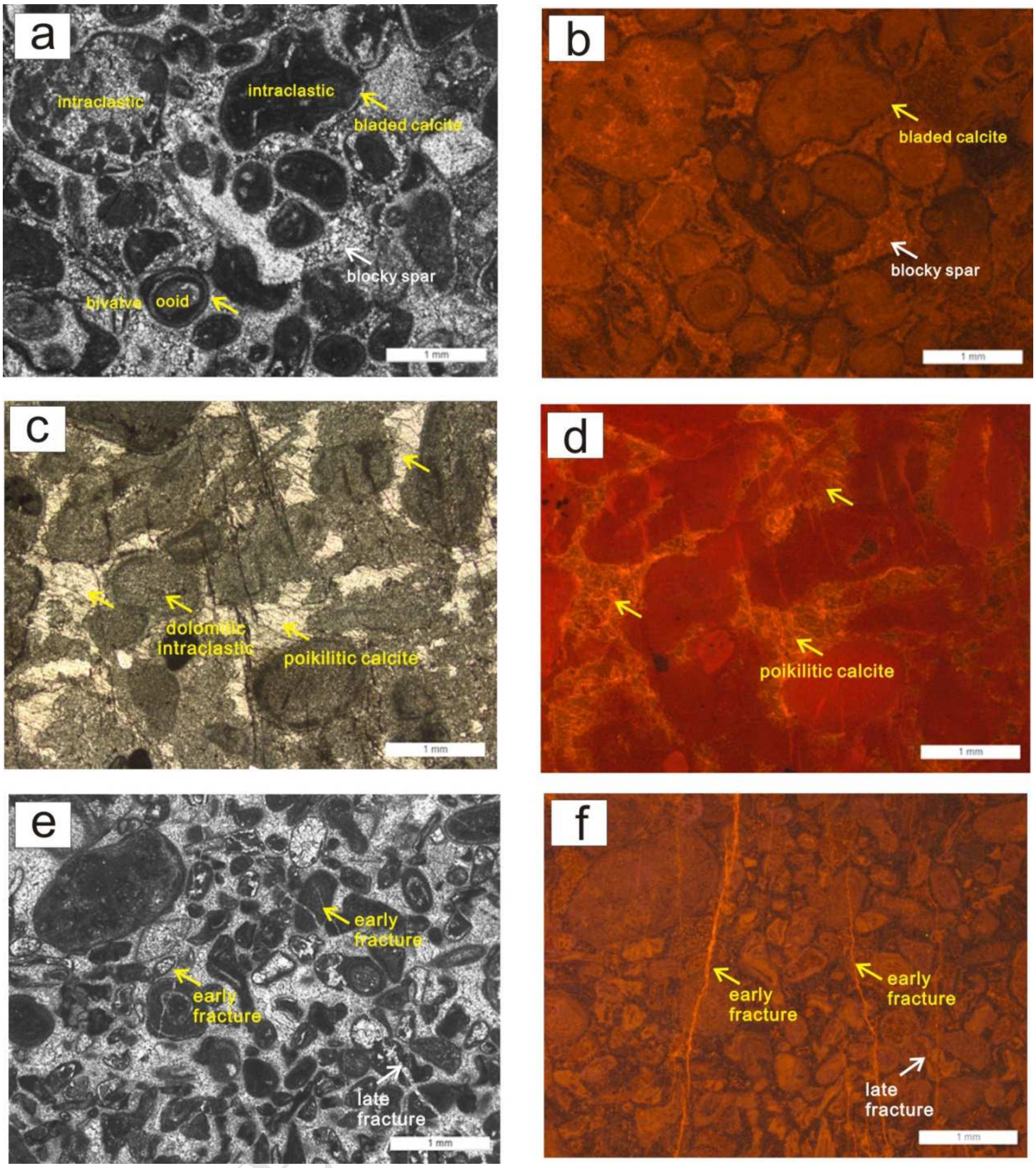

Fig.3 Lithology of the Xiaohaizi Formation **(a).** Intrasparite limestone containing ooids, intraclast, and bioclast under plane-polarized light. The dark colours of grains were related to organic matters. The two generations of calcite cementation obstruct nearly all visible pores. **(b).**The image of (a) under cathode luminescence (CL). Note the CL colours of two generations of calcite cements are different. The early bladed calcites are non-luminescent, while the late blocky spars are dull orange. **(c)**.Fine crystalline intraclastic dolostone, cemented by poikilotopic calcite, under plane-polarized light. The crystals of dolomite are dull yellow. **(d)**.The image of (c) under CL. The CL colours of complete dolomitized grains are subtle null, while the poikilotopic calcites have dark orange colours. **(e)**. Intrasparite limestone with two phases of micro-fractures, under plane-polarized light. **(f)**. the image of (e) under CL. The CL colours of early micro-fractures are bright orange, while that of the late fracture are dark orange.

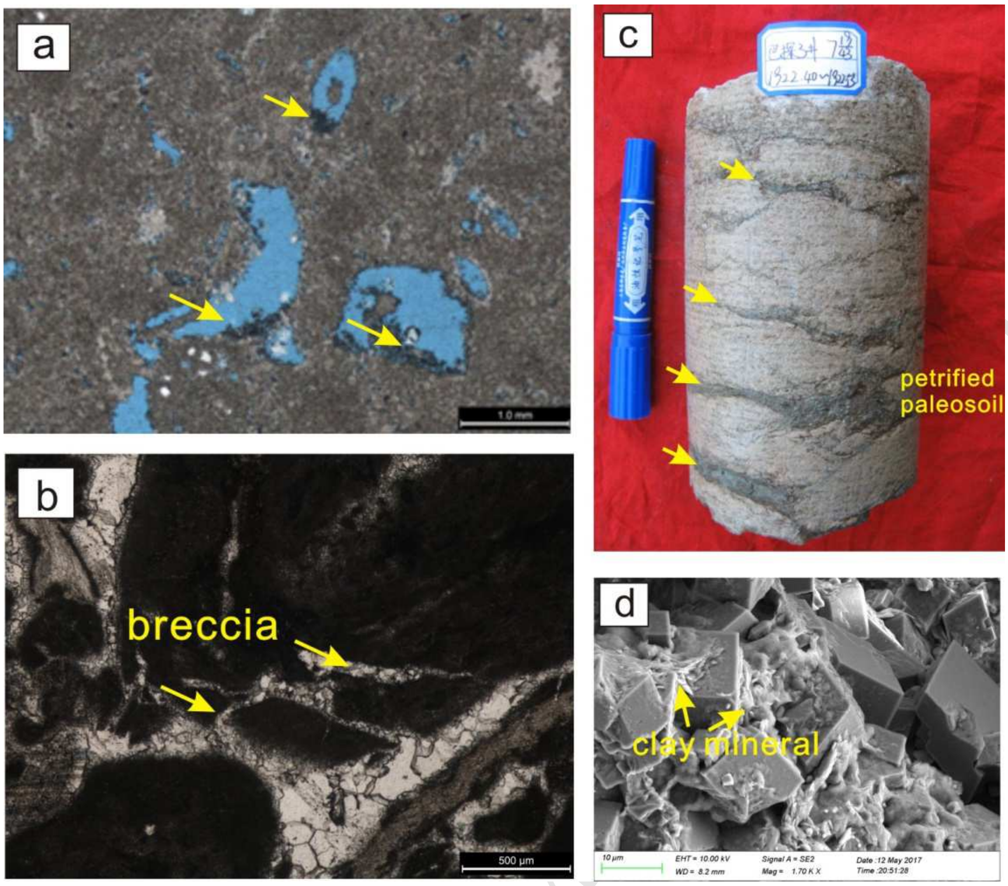

Fig.4 The features of subaerial exposure. **(a).** Vadose silt filled in the moldic pores of bioclast. VS-vadose silt. **(b).** Weathering breccia in intrasparite limestone, cemented by calcites. Br-breccia. **(c).** Several palaeosol layers on the brecciated dolostone in the lower Xiaohaizi Formation, indicated by yellow arrows. **(d)**. SEM image of clay minerals among dolomites.

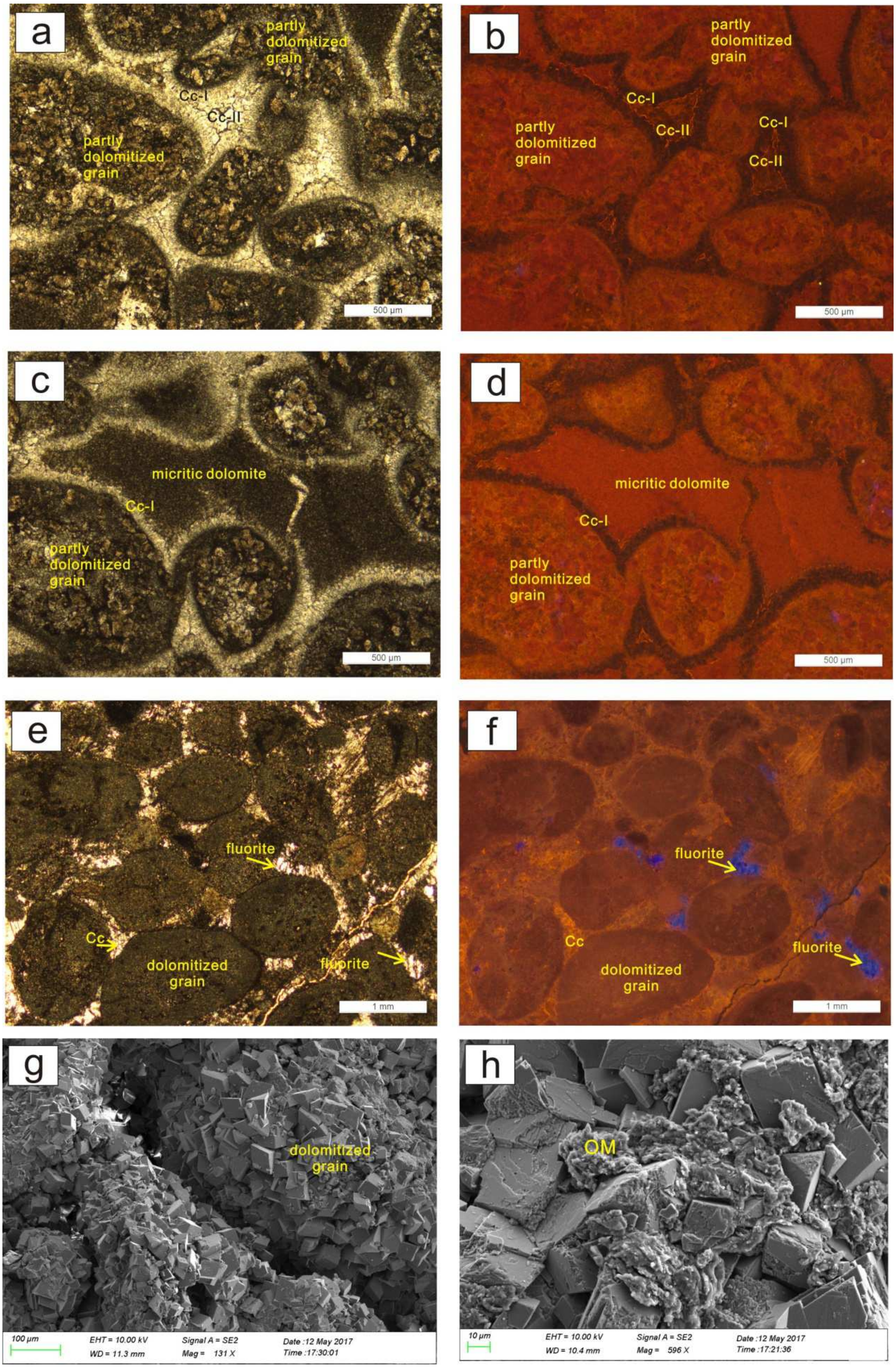

Fig.5 The features of dolomitization in the Xiaohaizi Formation. **(a)**.Dolomitic intrasparite limestone with partly dolomitized grains, under plane-polarized light. The

crystals of dolomite inside grains are dirty and fine. The two generations of calcite cements obstructed nearly all visible pores. Cc-calcite; Cc-I-the first generation of calcite; Cc-II-the second generation of calcite; **(b)**. The image of (a) under cathode luminescence (CL). Partially dolomitized grains have dark red colours under CL, minor dark orange. The CL colours of early bladed calcites are dull, caused by very low Mn^{2+}. The late blocky calcites have dark orange colours under CL, indicating a low Mn^{2+} or high Fe^{2+} diagenetic environment. **(c).** Dolomitic intramicrite, under plane-polarized light. The grains have partly dolomitized, while the matrix is completely dolomitized. The bladed calcites grow around grains as isopachous fringes. **(d).** The image of (c) under CL. The partly dolomitized grains have weak orange colours. The colours of bladed calcite are null, while the micritic dolomites have weak red colours. **(e)**. Intraclastic dolostone, under plane-polarized light. The dolomitized grains are dark earthy yellow. Poikilotopic calcites and fluorites fill in the pores. **(f).** The image of (e) under CL. The colours of complete dolomitized grains are subtle dull, indicating a very low Mn^{2+} environment. Poikilotopic calcites have dark to bright orange colours. The fluorites have deep blue colours. **(g)**. The SEM image of dolomitized grains, with the crystal size ranging from14-32μm. **(h).** The SEM image of organic matters among dolomites. These organic matter contain abundant C, N, O, belonging to the component of palaeosol. OM-organic matter.

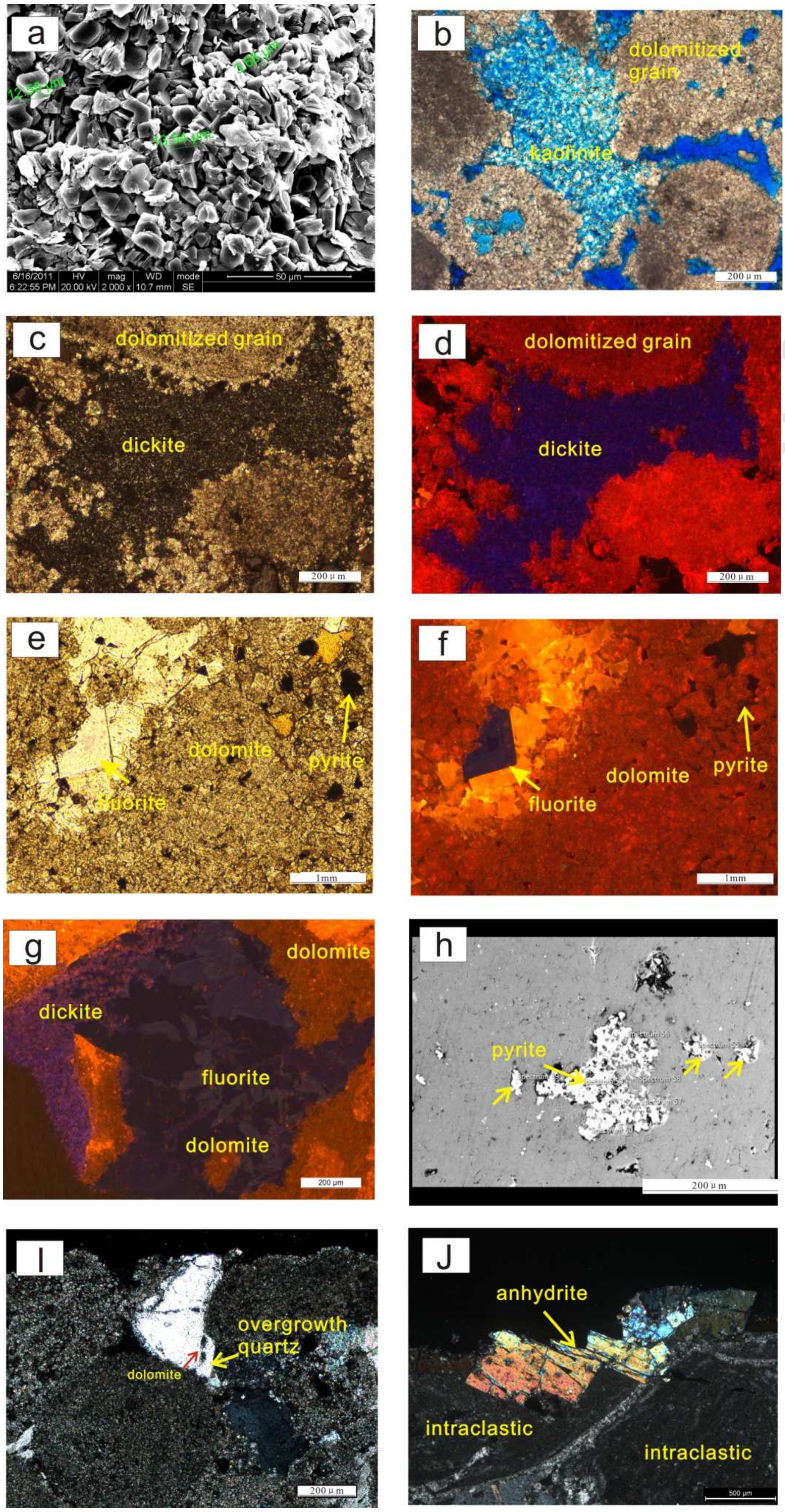
a
6/16/2011 HV mag WD mode 50 μm
6:22:55 PM 20.00 kV 2 000 x 10.7 mm SE
b
dolomitized grain
kaolinite
200 μ m
c
dolomitized grain
dickite
200 μ m
d
dolomitized grain
dickite
200 μ m
e
dolomite
pyrite
fluorite
1mm
f
dolomite
pyrite
fluorite
1mm
g
dolomite
dickite
fluorite
dolomite
200 μm
h
pyrite
200 μ m
I
overgrowth quartz
dolomite
200 μ m
J
anhydrite
intraclastic
intraclastic
500 μm

Fig.6 The photos of diagenetic minerals in the Xiaohaizi Formation. **(a).** The SEM image of dickites. The blocky dickite crystals, with size of 3-13μm, have the spatial organization seems inherited from pre-existing booklets. **(b).** The image of kaolinites filling in intergranular dissolved pores among dolomitized grains, under plane-polarized light. Blue areas are pores. **(c).** Dickites fill within intergranular dissolved pores, under cross-polarized light. Dickites have interference colour of greyish white. **(d).** The image of (c) under cathode luminescence (CL). Dickites have deep blue colours under CL. The dissolved dolomites were enclosed by dickites. **(e).** Euhedral crystal of fluorite grows in dolostone. Opaque pyrites are oserved. **(f).** The image of (e) under CL. The colour of fluorite is bluish-violet. **(g).** The image of fluorites and dickites under CL, from Fu et al., 2012b. The dickites were enclosed in fluorites, indicating precipitation of fluorites postdated dickites. **(h).** The SEM image of pyrite on thin section. Authigenic pyrite filled in the dissolved pores, postdating dissolution. **(I).** The image of overgrowth quartz under cross-polarized light. The overgrowth quartz grows towards intergranular pores. It shows quartz overgrowth occurred after compaction. There are fine crystals of dolomite existing between detrital quartz and overgrowth quartz. **(J).** The image of anhydrite in the partly dolomitized intrasparite under cross-polarized light. The bright interference colour and plate like structure can be identified as anhydrite.

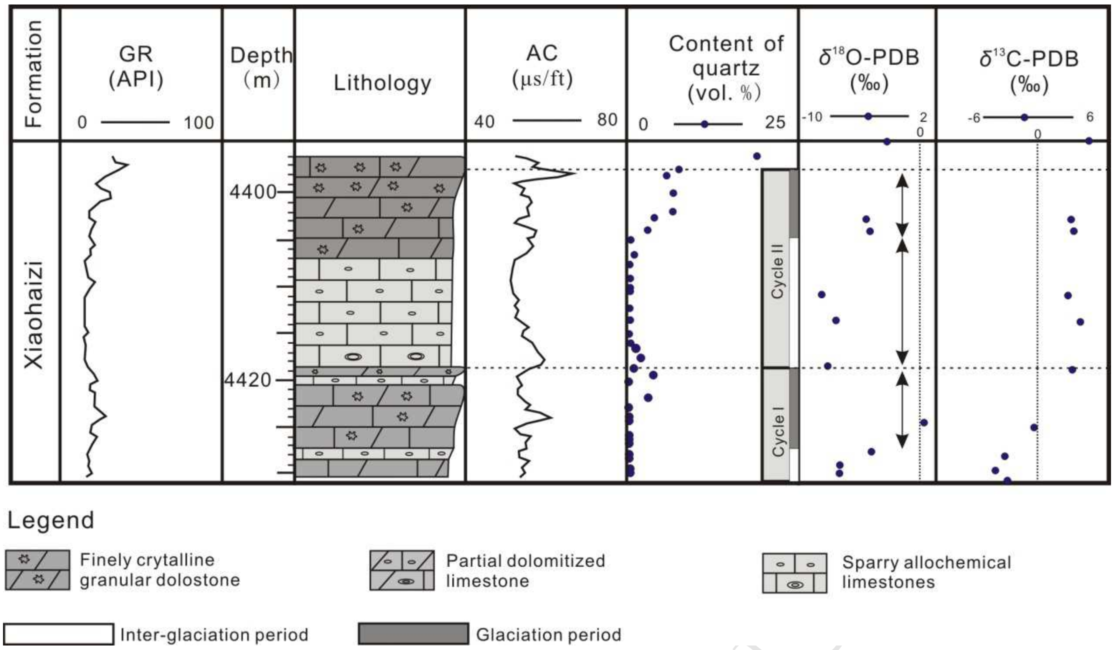

Fig.7 The vertical variation of content of terrigenous quartz, carbon and oxygen isotope of the Xiaohaizi Formation in well M10. Note that there are two cycles of inter-glaciation period and glaciation period. The high content of quartz and enrichment of ^{18}O stands for the onset of glacial period.

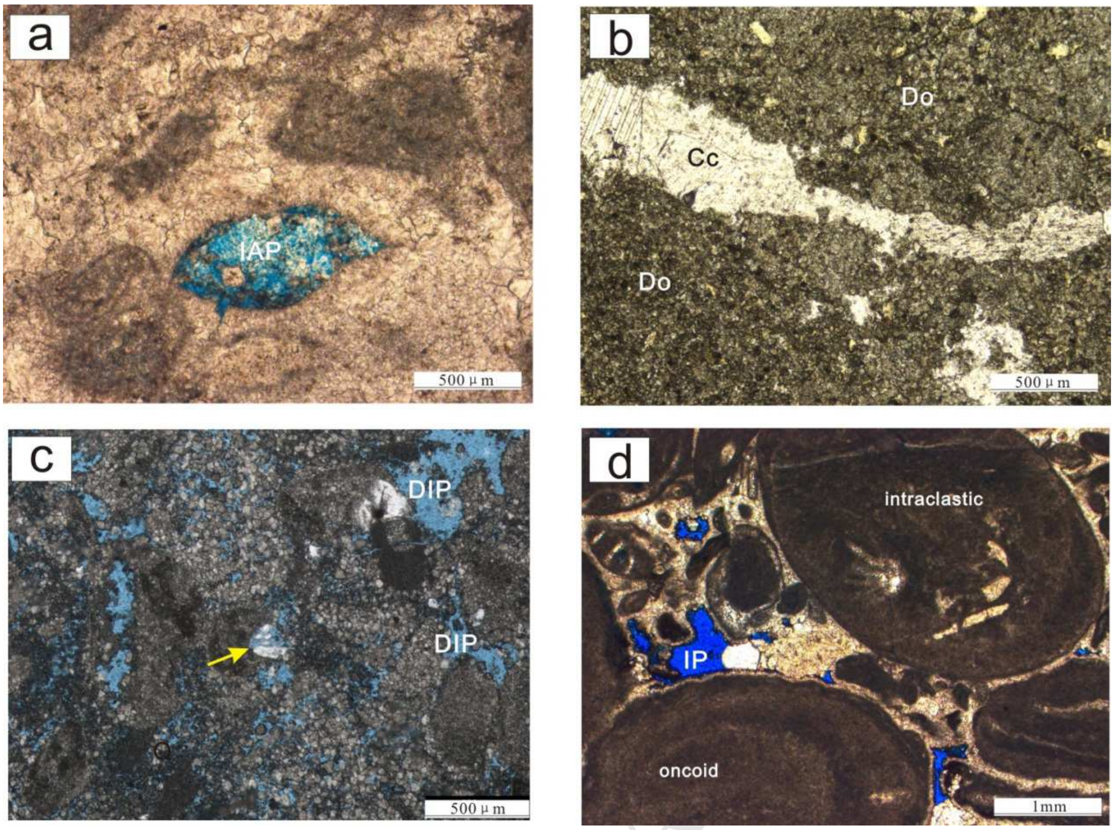

Fig.8 The photos of different types of pores in the Xiaohaizi Foramtion. **(a).** The image of intragranular pore under plane-polarized light. **(b).** The non-fabric selective pores filled with calcite, under plane-polarized light. **(c).** The image of dissolved intergranular pores, under plane-polarized light. Paritally dissolved feldspar (yellow arrow) is present. **(d).** The image of primary intergranular pores in intrasparite, under plane-polarized light. DIP: dissolved intergranular pore; IP: intergranular pore; IAP: intragranular pore; Cc: calcite; Do: dolomite.

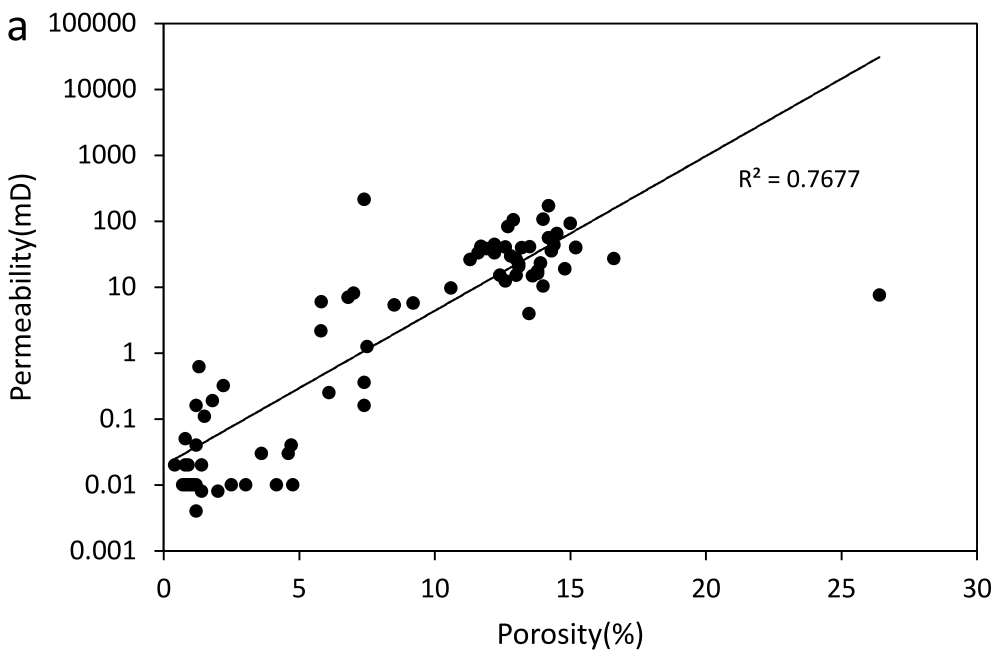

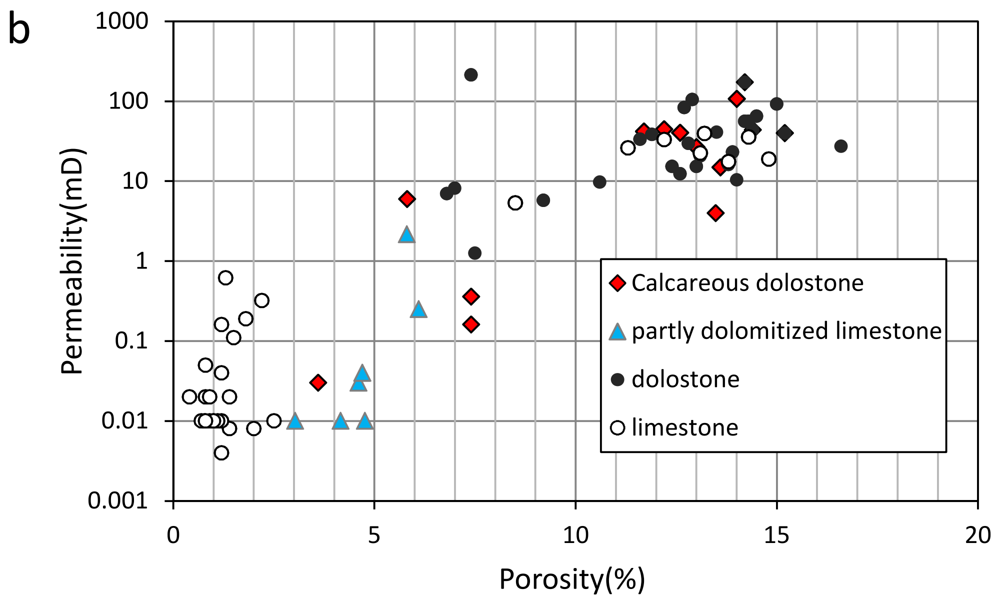

Fig.9 The cross plots of porosity and permeability. **(a).**The bulk data for all samples. There is a good positive correlation, with coefficient of 0.7677. **(b).** The relationship between lithology and physical property. The dolostones have highest porosity and permeability than other rocks.

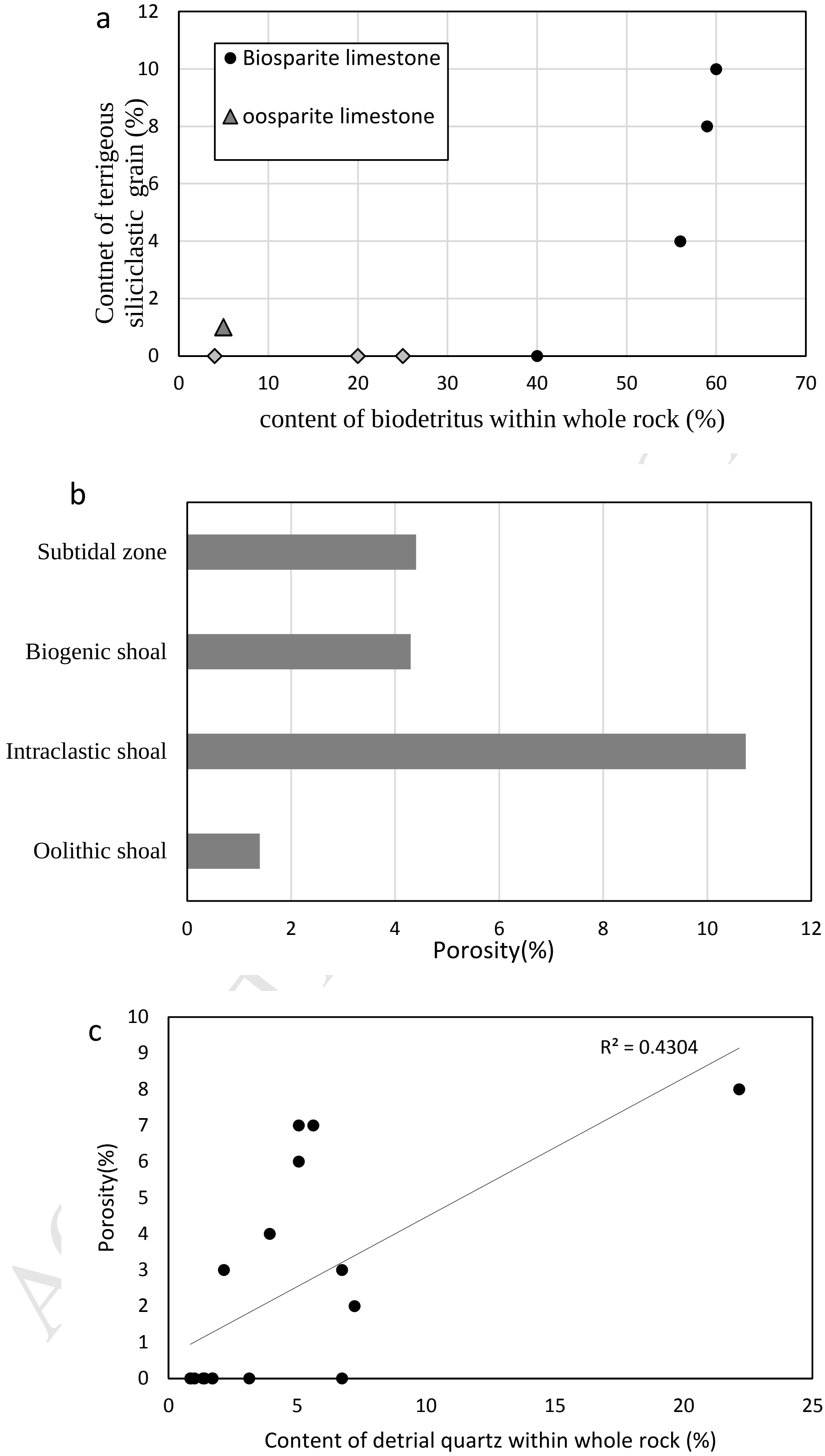
a
Biosparite limestone
oosparite limestone
Contnet of terrigeous siliciclastic grain (%)
content of biodetritus within whole rock (%)
0
2
4
6
8
10
12
0
10
20
30
40
50
60
70
b
Subtidal zone
Biogenic shoal
Intraclastic shoal
Oolithic shoal
0
2
4
6
8
10
12
Porosity(%)
c
R² = 0.4304
Porosity(%)
Content of detrial quartz within whole rock (%)
0
1
2
3
4
5
6
7
8
9
10
0
5
10
15
20
25

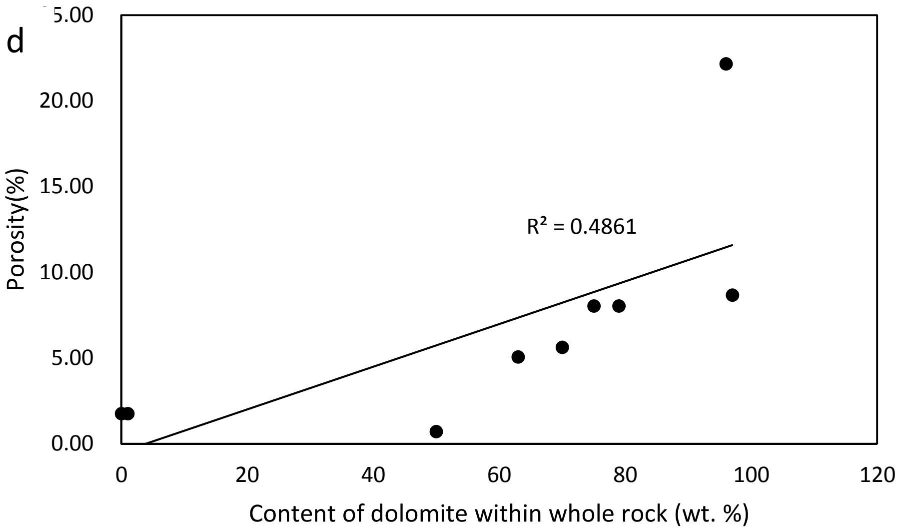

Fig.10 The correlation analysis of physical property, lithology and rock components. **(a).** The cross plot of terrigenous grains contents and biodetritus contents within whole rock; **(b).** The porosities of reservoir rocks from different microfacies of carbonate shoals; **(c).** The cross plot of porosities of reservoir rocks and contents of detrial quartz within whole rock; **(d).** The cross plot of porosities of reservoir rocks and contents of dolomite within whole rock.

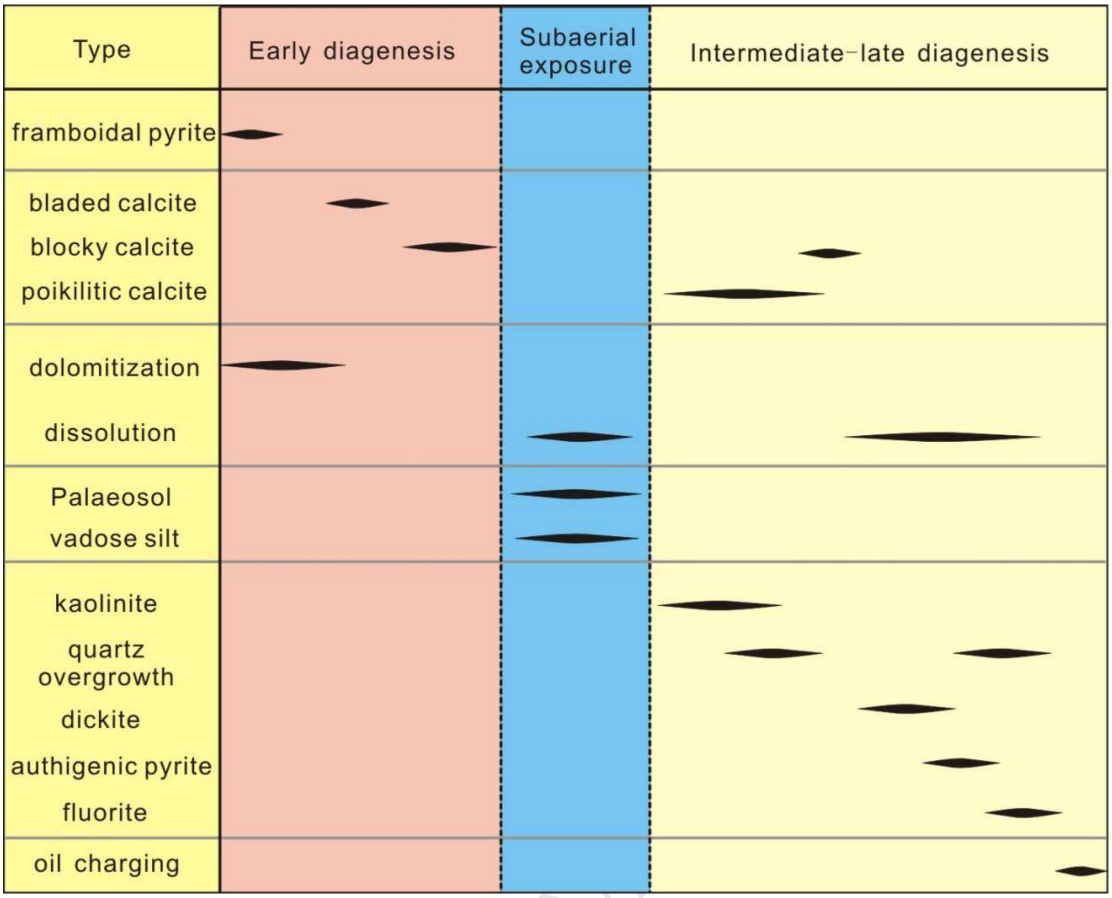

Fig.11 Paragenesis of the carbonate rocks from the Xiaohaizi Formation

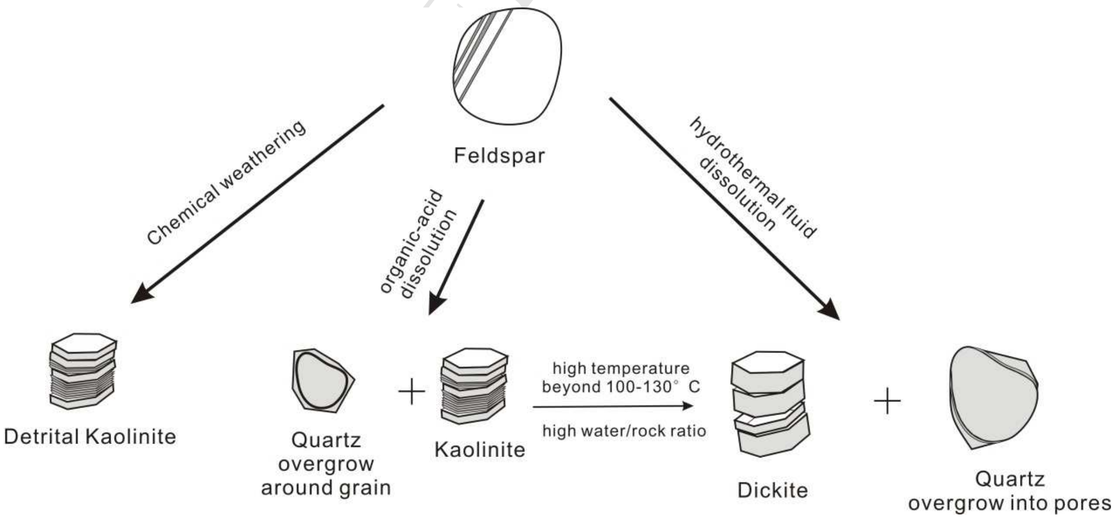

Fig.12 The transformation pathway of kaolinite and dickite in the Xiaohaizi Formation

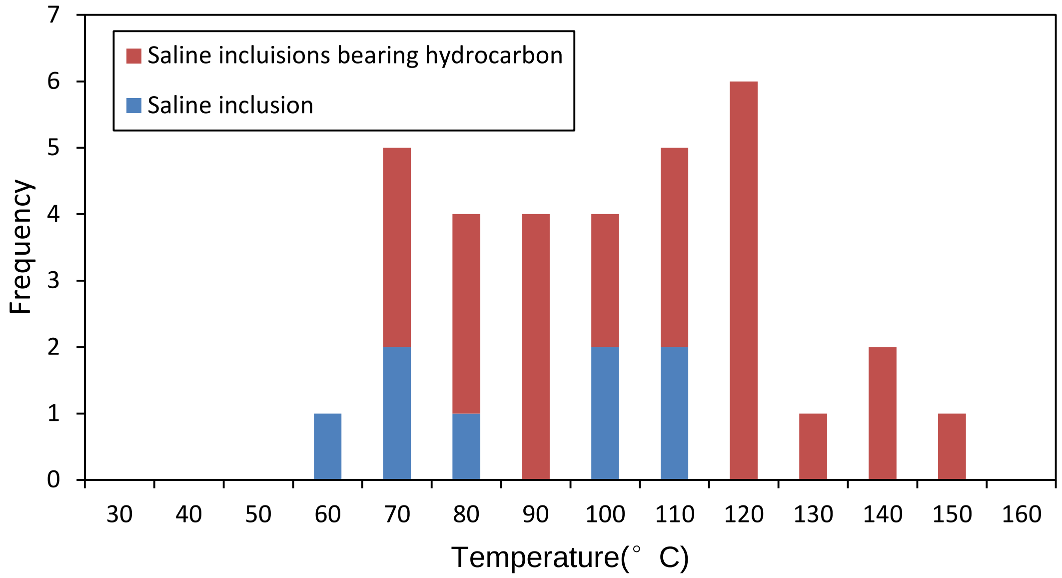

Fig.13 The homogeneous temperatures of fluid inclusions within the calcite veins of the Xihaozi Formation in well BT4.

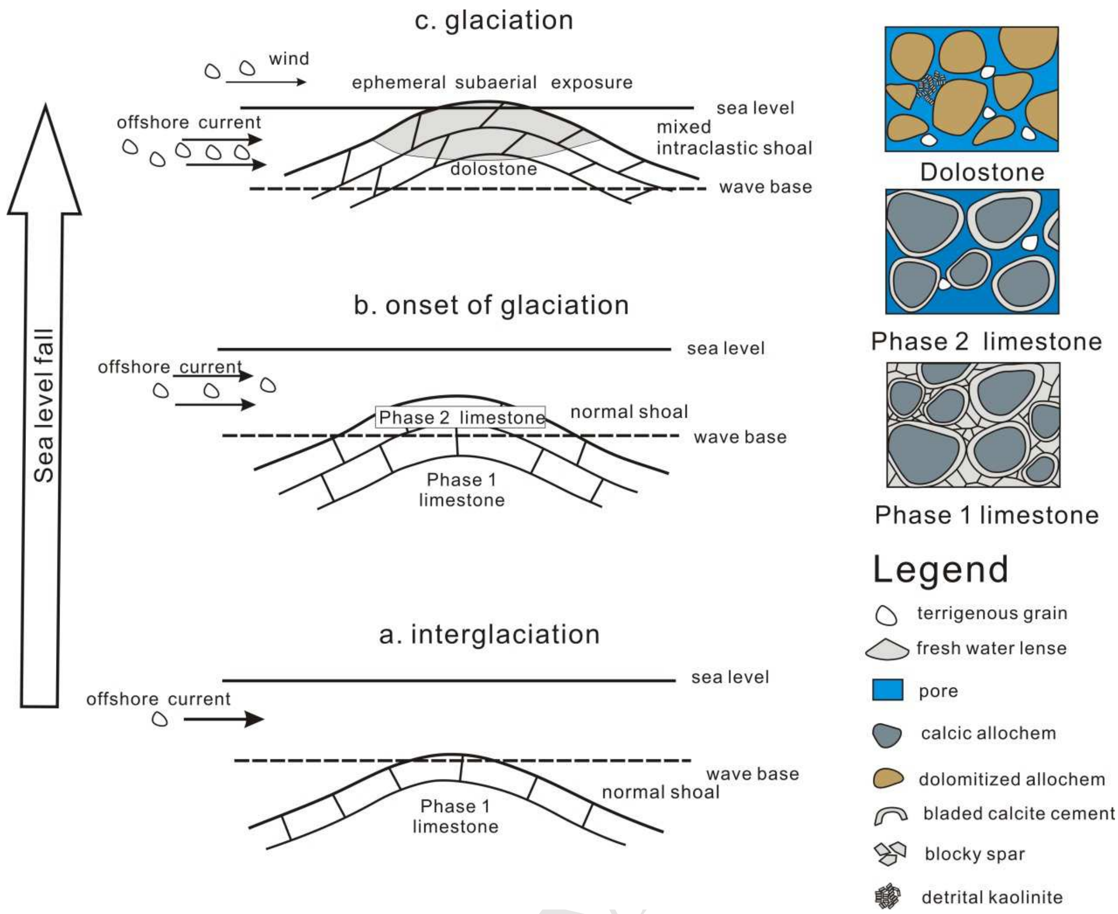

Fig.14 The depositional and diagenetic model of the Xiaohaizi Formation during the cycle of interglaciation and glaciation. The mixed siliciclastic-carbonate sedimentation and subaerial exposure controls the formation of porous dolostones, as response to the sea level fall with proceeding of glaciation. Dolostones with weak cementation have abundant pores to be the best reservoir rocks.

(1) The mixed sedimentation on the carbonate shoals could influence the physical property of reservoirs.

(2) Reservoir quality was controlled by mixed sedimentation and dolomitization associated with glacio-eustatic fluctuation.

(3) Evidences for the emergence of dolostones include vadose silt. palaeosol, karst breccia, detrital kaolinite, darkening of dolostones, and positive $\delta^{18}O_{-carbonate}$.